Aspen Tension Wood Fibers Contain β-(1→4)-Galactans and Acidic Arabinogalactans Retained by Cellulose Microfibrils in Gelatinous Walls[1][OPEN]

Tatyana Gorshkova*, Natalia Mokshina, Tatyana Chernova, Nadezhda Ibragimova, Vadim Salnikov, Polina Mikshina, Theodora Tryfona, Alicja Banasiak, Peter Immerzeel, Paul Dupree, and Ewa J. Mellerowicz*

Kazan Institute of Biochemistry and Biophysics, Kazan Scientific Centre, Russian Academy of Sciences, 420111 Kazan, Russia (T.G., N.M., T.C., N.I., V.S., P.M.); Department of Biochemistry, University of Cambridge, Cambridge CB2 1QW, United Kingdom (T.T., P.D.); Department of Forest Genetics and Plant Physiology, Swedish University of Agricultural Sciences, Umea Plant Science Centre, 90183 Umea, Sweden (A.B., P.I., E.J.M.); and Institute of Experimental Biology, University of Wroclaw, 50–328 Wroclaw, Poland (A.B.)

ORCID IDs: 0000-0003-0342-8195 (T.G.); 0000-0002-2367-672X (V.S.); 0000-0001-9270-6286 (P.D.); 0000-0001-6817-1031 (E.J.M.).

Contractile cell walls are found in various plant organs and tissues such as tendrils, contractile roots, and tension wood. The tension-generating mechanism is not known but is thought to involve special cell wall architecture. We previously postulated that tension could result from the entrapment of certain matrix polymers within cellulose microfibrils. As reported here, this hypothesis was corroborated by sequential extraction and analysis of cell wall polymers that are retained by cellulose microfibrils in tension wood and normal wood of hybrid aspen (*Populus tremula* × *Populus tremuloides*). β-(1→4)-Galactan and type II arabinogalactan were the main large matrix polymers retained by cellulose microfibrils that were specifically found in tension wood. Xyloglucan was detected mostly in oligomeric form in the alkali-labile fraction and was enriched in tension wood. β-(1→4)-Galactan and rhamnogalacturonan I backbone epitopes were localized in the gelatinous cell wall layer. Type II arabinogalactans retained by cellulose microfibrils had a higher content of (methyl)glucuronic acid and galactose in tension wood than in normal wood. Thus, β-(1→4)-galactan and a specialized form of type II arabinogalactan are trapped by cellulose microfibrils specifically in tension wood and, thus, are the main candidate polymers for the generation of tensional stresses by the entrapment mechanism. We also found high β-galactosidase activity accompanying tension wood differentiation and propose a testable hypothesis that such activity might regulate galactan entrapment and, thus, mechanical properties of cell walls in tension wood.

Contractile cell walls found in plant organs and tissues such as tendrils, contractile roots, and tension wood (TW) have remarkable functions and properties. Their traits have been most intensely studied in TW of hardwoods, where they provide negative gravitropic response capacities to stems with secondary growth, as recently reviewed by Mellerowicz and Gorshkova (2012). These properties are conferred by TW fibers, which in many species contain a so-called gelatinous cell wall layer (G-layer; Norberg and Meier, 1966; Clair et al., 2008). G-layers are formed following the deposition of xylan-type secondary cell wall layer(s) and, thus, can be considered tertiary layers (Wardrop and Dadswell, 1948). They are almost or completely devoid of xylan and lignin and have very high cellulose contents (up to 85%). However, several other polymers appear to be present in TW G-layers, according to recent chemical analyses of isolated G-layers (Nishikubo et al., 2007; Kaku et al., 2009) and immunohistochemical labeling of TW sections (Arend, 2008; Bowling and Vaughn, 2008). Notably, xyloglucan (XG) has been found in G-layers of poplar (*Populus* spp.) TW (Nishikubo et al., 2007) and at the boundary between secondary cell wall layers

[1] This work was supported by the Swedish Governmental Agency for Innovation Systems, the Swedish Research Council, the Russian Foundation for Basic Research (grant nos. 15–04–02560 and 15–04–05721), and the Biotechnology and Biological Sciences Research Council (grant no. BB/G016240/1 and funds from the Sustainable Energy Centre Cell Wall Sugars Programme).

* Address correspondence to gorshkova@kibb.knc.ru and ewa.mellerowicz@slu.se.

The author responsible for distribution of materials integral to the findings presented in this article in accordance with the policy described in the Instructions for Authors (www.plantphysiol.org) is: Ewa J. Mellerowicz (ewa.mellerowicz@slu.se).

T.G. designed the project, supervised the majority of the work, and wrote the article; N.M. performed the gel filtration chromatography and monosaccharide analysis; T.C. isolated and fractionated the cell walls; N.I. conducted the immunodot experiments; V.S. performed the electron microscopy with immunocytochemistry; P.M. analyzed the polymer structure by NMR spectroscopy; T.T. performed the PACE experiments; A.B. performed the in situ activity tests; P.I. isolated and prepared material for the biochemical analyses; P.D. supervised the PACE experiments; E.J.M. designed the project outline, supervised part of the work, and revised the article; all authors contributed to the article writing and approved the final content.

[OPEN] Articles can be viewed without a subscription.
www.plantphysiol.org/cgi/doi/10.1104/pp.15.00690

(S-layers) and G-layers (Baba et al., 2009; Sandquist et al., 2010). It is also important for tension creation (Baba et al., 2009). However, it is not detectable in mature G-layers by monoclonal antibodies or XG-binding modules (Nishikubo et al., 2007; Baba et al., 2009; Sandquist et al., 2010).

Structurally similar G-layers have been also identified in phloem fibers in many fibrous crops, such as flax (*Linum usitatissimum*), hemp (*Cannabis sativa*), and ramie (*Boehmeria nivea*; Gorshkova et al., 2012). These fibers occur in bundles that can be isolated for biochemical analysis. G-layers in fibers from diverse sources have a very similar structure, being largely composed of cellulose (with axial microfibril orientation, high degrees of crystallinity, and large crystallite sizes) lacking xylan and lignin (Mellerowicz et al., 2001; Pilate et al., 2004; Gorshkova et al., 2010, 2012) and having high water contents (Schreiber et al., 2010). In phloem fibers, the G-layers become very prominent, reaching thicknesses up to 15 μm and occupying over 90% of the cell wall's total cross-sectional areas (Crônier et al., 2005). Pectic β-(1→4)-galactan with complex structures has been shown to be the major matrix polysaccharide of isolated phloem fibers in flax (Gorshkova et al., 2004; Gorshkova and Morvan, 2006; Gurjanov et al., 2007). Some of it is so strongly retained within cellulose that it cannot be extracted by concentrated alkali and can only be obtained after cellulose dissolution (Gurjanov et al., 2008). Such galactan, therefore, is a prime candidate for a polymer entrapped by cellulose microfibrils during crystallization that could substantially contribute to the contractile properties of cellulose in G-layers, according to recently formulated models (Mellerowicz et al., 2008; Mellerowicz and Gorshkova 2012). Furthermore, Roach et al. (2011) have shown that trimming of β-(1→4)-galactan by β-galactosidase is important for final cellulose crystallization, the formation of G-layer structure, and, hence, the stem's mechanical properties.

There is also immunocytochemical evidence for the presence of β-(1→4)-galactan and type II arabinogalactan (AG-II) in G-layers of TW fibers (Arend, 2008; Bowling and Vaughn, 2008). In addition, high-M_r branched galactans have been isolated from TW of *Fagus sylvestris* (Meier, 1962) and *Fagus grandifolia* (Kuo and Timell, 1969), with estimated degrees of polymerization (DP) of approximately 300 and complex structure, probably including both β-(1→4) and β-(1→6) linkages, although their exact nature remains unknown. Furthermore, Gal has been identified as one of the major sugars after Glc and Xyl in hydrolysates of isolated *Populus* spp. G-layers (Furuya et al., 1970; Nishikubo et al., 2007), and the Gal content of cell walls is a proposed indicator of the extent of TW development in beech (*Fagus* spp.; Ruel and Barnoud, 1978). However, subsequent linkage analyses identified only 2- and 3,6-linked Gal in poplar TW G-layers (Nishikubo et al., 2007), while in flax fibers, 4-linked Gal is the main component (Gorshkova et al., 1996, 2004; Gurjanov et al., 2007, 2008). Thus, the type(s) of galactans present in poplar TW remains unclear, and the galactans have not been shown previously either to have a rhamnogalacturonan-I (RG-I) backbone or to be strongly retained by cellulose microfibrils, as demonstrated for flax gelatinous fibers.

To improve our understanding of cell wall properties in TW and their contraction mechanism, in the study presented here, we tested aspects of the recently proposed entrapment model (Mellerowicz et al., 2008; Mellerowicz and Gorshkova, 2012). According to this model, contraction is driven by the formation of larger cellulose structures, sometimes called macrofibrils, via interactions of cellulose microfibrils in the G-layer with each other and forming inclusions containing matrix polymers. This would induce tension within cellulose through the stretching of microfibrils required to surround the inclusions. The model is compatible with available data on the structure and action of gelatinous walls, but the main assumption, that polymers are trapped inside crystalline cellulose, such as that found in flax, has not been tested previously. Therefore, we compared matrix polymers retained by cellulose microfibrils in normal wood (NW) and TW of the model hardwood species hybrid aspen (*Populus tremula* × *Populus tremuloides*) that forms TW with gelatinous fibers. For this purpose, we used a combination of sequential cell wall extractions, similar to those used previously to characterize flax gelatinous fibers (Gurjanov et al., 2008), followed by fractionation of polymers by size-exclusion chromatography, immunological analyses, and oligosaccharide profiling by polysaccharide analysis using carbohydrate gel electrophoresis (PACE). The results reveal the main polymers of cellulose-retained fractions and key differences between NW and TW. Comparison of our results and previous findings also indicates that there are both similarities and differences in the constitution of gelatinous fibers in aspen and flax. An updated model of the contractile G-layer of TW fibers based on the data is presented.

RESULTS

Sequential Cell Wall Extraction and Analysis Reveals Basic Differences between NW and TW

To induce TW, aspen trees were tilted at approximately 45° from vertical for several weeks. This induced the formation of gelatinous fibers with very prominent G-layers, while fibers in NW of upright control trees predominantly had solely secondary walls (Fig. 1A). After milling to the same particle size, TW and NW samples had distinct textures (Fig. 1B). Monosaccharide analysis of total trifluoroacetic acid (TFA)-hydrolyzable sugars in cell walls of these samples revealed that TW had considerably lower proportions of Xyl (although it remained the major sugar) and Man than NW (Fig. 1C). In contrast, the proportion of Glc (the second most abundant monomer in the hydrolysates), which could at least partly originate from amorphous cellulose and XG, was higher in TW (203 ± 30 mg g^{-1} dry weight) than in NW (110 ± 32 mg g^{-1} dry weight). Proportions

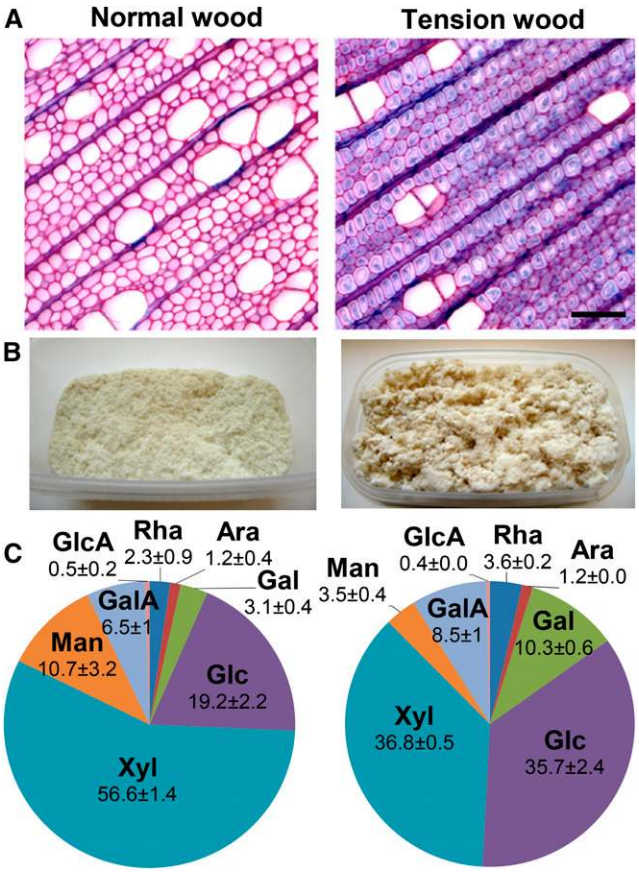

Figure 1. Anatomy, macroscopic appearance, and monosaccharide composition of NW and TW. A, Light microscopy images of NW from an upright tree and TW from a tilted tree stained with Alcian Blue-safranin. Note the prominent nonlignified G-layers stained blue in TW and the lignified compound middle lamella and S-layers stained red in both NW and TW. Bar = 50 μm. B, Appearance of NW and TW after milling. C, Monosaccharide composition (mol %) of TFA hydrolysates of NW and TW.

of Gal, Rha, and GalA were also higher in TW than in NW.

To characterize cell wall polysaccharides more specifically, NW and TW samples were fractionated by the sequential extraction procedure shown in Supplemental Figure S1 into buffer-soluble polymers, ammonium oxalate (AO)-extractable polymers, 4 M KOH-extractable polymers, cellulose-retained polymers, lignin-bound polymers, and lignin. Yields of the fractions obtained from NW and TW differed considerably (Table I), but cellulose, KOH-extractable polymers, and lignin were the most abundant fractions in both cases. As expected, KOH-extractable polymers and lignin contents were lower, while cellulose contents were higher, in TW than in NW. Buffer-extractable polymers were also considerably more abundant (but still a minor fraction) in TW. The cellulose-retained non-Glc polymers constituted approximately 2% of cell wall dry weight in both wood types.

To gain an oversight of the composition of polysaccharides in the fractions, their monosaccharide compositions were first determined (Tables II and III). The major constituents of the buffer-soluble fraction, according to monosaccharide analysis, were Gal, Rha, and GalA, suggesting the presence of pectic galactan. In both wood types, the 4 M KOH fraction contained mostly Xyl, which was initially measured together with Man [Xyl(Man)]. However, its content was lower in TW (Tables II and III). Separation of Xyl and Man in further subsequent analysis of the fraction indicated that Man constituted around 12% of Xyl(Man) in both NW and TW. TFA hydrolysis of the non-KOH-extractable cell wall material yielded mainly Glc. Non-Glc monosaccharides of this fraction amounted to 19 $\pm$ 3 and 22 $\pm$ 6 mg g^{-1} dry weight in NW and TW, respectively, Xyl (Man) accounting for approximately half of these amounts. Gal was the next most abundant sugar in TW samples, in which its proportion was twice as high as in NW (Tables II and III). Cellulose-retained matrix polysaccharides (excluding Glc) contributed around one-third of the total yield of monosaccharides from the KOH-unextractable fraction and amounted to 7 $\pm$ 2 and 8 $\pm$ 4 mg g^{-1} dry weight in NW and TW samples, respectively. Gal was twice as abundant in polymers of this fraction from TW as in corresponding polymers from NW in both absolute amounts and proportions (35 $\pm$ 3 versus 17 $\pm$ 2 mol %; Tables II and III). Some carbohydrates (5 $\pm$ 2 and 3 $\pm$ 1 mg g^{-1} dry weight in NW and TW, respectively) remained in the pellet after all the applied extraction procedures and were presumably linked to lignin. The yield of this fraction was lower from TW samples, mainly due to reductions in Glc amounts, while proportions of other sugars in the TW and NW fractions were similar (Tables II and III).

The fractions were subsequently subjected to immunodot analysis using antibodies recognizing cell wall matrix polysaccharides likely to be present according to their monosaccharide compositions. These were LM11 for β-(1→4)-xylan (McCartney et al., 2005), LM15 for XG (Marcus et al., 2008), JIM14 for arabinogalactan protein (AGP; Knox et al., 1991), LM5 for β-(1→4)-galactan (Jones et al., 1997), and RU2 for RG-I backbone (Ralet et al., 2010). Sugar contents of samples of total fractions were equalized, and the samples were used in several dilutions. Images of the membrane with immunodots obtained for buffer-soluble, KOH-extractable, and cellulose-retained polysaccharides are presented in Figure 2. Most β-(1→4)-xylan, as indicated by LM11 antibody binding, was extracted by 4 M KOH, some appeared in the cellulose-retained fraction, but none was detected in the buffer-soluble fraction. Xylan signals were weaker in the KOH-extractable fraction of TW than in the corresponding NW fraction but were similar in the cellulose-retained fraction of both wood types. JIM14 labeling, indicative of arabinogalactan, appeared in all analyzed fractions, but more strongly in NW than in TW samples. LM15 labeling indicated the presence of trace amounts of XG in the KOH-extractable fraction of NW and greater amounts in this fraction of TW. There was also a trace of XG in the cellulose-retained fraction of TW but not NW.

Table I. *Yields of cell wall fractions in NW and TW*

Data are means ± SE (n = 3).

Fraction	NW	TW
	mg g^{-1} dry wt	
Buffer-extractable polymers[a]	1 ± 0	8 ± 1
AO-extractable polymers[a]	3 ± 0	2 ± 0
KOH-extractable polymers[a]	217 ± 22	126 ± 14
KOH-unextractable material (hydrolyzable by TFA without Glc)[b]	19 ± 3	25 ± 7
Lignin[c]	211 ± 16	109 ± 12
Cellulose[d]	549 ± 20	730 ± 26

[a]Determined as sugar content by the phenol-sulfuric acid method (Dubois et al., 1956). [b]Determined as the sum of yields of all monosaccharides obtained by TFA hydrolysis from the pellet remaining after AO and KOH treatments. [c]Calculated by subtracting yields of all monosaccharides obtained by TFA hydrolysis from the pellet remaining after the removal of KOH-unextractable matrix polymers and cellulose. [d]Calculated from the dry mass of the initial sample by subtracting yields of buffer-extractable, AO-extractable, KOH-extractable, and KOH-unextractable polysaccharides and lignin.

Immunodot analysis with LM5 revealed higher amounts of β-(1→4)-galactan in TW than in NW samples in all analyzed fractions (but particularly the cellulose-retained fraction), and this was the most significant difference between them. Immunolabeling with RU2 antibody confirmed the presence of RG-I backbone in all analyzed fractions, and RU2 signal was substantially stronger in the cellulose-retained fraction of TW than in the corresponding NW fraction.

These results indicate three major differences between NW and TW. TW contains more buffer-soluble polymers and cellulose but less hemicelluloses and lignins (Table I; Fig. 1). There are differences in monomeric composition between NW and TW in all of the fractions (corroborated by the observed differences in immunolabeling with specific antibodies). And TW samples (of all fractions) appear to contain significantly higher levels of β-(1→4)-galactan.

Size-Exclusion Chromatography Fractionation of Different Extracts and Characterization of Subfractions Reveal Differences in Galactans between NW and TW

To compare mass distributions of polymers in NW and TW samples, the polysaccharide fractions were subjected to gel filtration, divided into high- and low-M_r subfractions according to the major peaks, and then analyzed in more detail.

Buffer-Soluble Polymers

The buffer-soluble fraction had substantial polymer contents in TW but very low contents in NW samples. The polymers purified by precipitation eluted in the 10- to 200-kD region (Fig. 3A), with a considerable proportion of carbohydrates present in the oligomeric region (less than 5 kD). Gal was the major monomer of the polymeric fraction, and its proportion was higher in TW than in NW (Fig. 3B). The oligomeric TW subfraction contained mostly Gal, GalA, and Rha, suggesting enrichment in RG-I oligosaccharides. Results of the sugar composition (Tables II and III) and immunodot analyses (Fig. 2) indicate that the main polymer of the buffer-soluble fraction in TW is high-M_r β-(1→4)-galactan. Some AG-II and oligomeric RG-I were also detected.

Table II. *Proportions of monosaccharides in fractions of TW and NW*

Data are means ± SE (n = 3 biological repeats). w/o, Without Glc, since Glc could have been derived from cellulose during the procedure used. Values with significant differences between NW and TW samples according to Student's t test ($P \leq 0.05$) are shown in boldface.

Fraction	Rha		Ara		Gal		Glc		Xyl(Man)		GalA		GlcA	
	NW	TW	NW	TW	NW	TW	NW	TW	NW	TW	NW	TW	NW	TW
	mol %													
Buffer-extractable polymers	**9 ± 2**	**13 ± 1**	8 ± 2	5 ± 2	**30 ± 3**	**51 ± 4**	10 ± 5	2 ± 1	**24 ± 8**	**2 ± 0**	**17 ± 3**	**27 ± 2**	**3 ± 1**	**1 ± 0**
AO-extractable polymers	**5 ± 1**	**11 ± 1**	**3 ± 0**	**6 ± 0**	13 ± 10	41 ± 16	**20 ± 5**	**8 ± 2**	**46 ± 9**	**11 ± 8**	**12 ± 2**	**21 ± 5**	1 ± 1	2 ± 0
KOH-extractable polymers	**2 ± 0**	**5 ± 0**	**1 ± 0**	**2 ± 0**	**2 ± 0**	**14 ± 2**	**4 ± 0**	**6 ± 1**	**83 ± 1**	**60 ± 4**	**8 ± 1**	**12 ± 1**	**0 ± 0**	**1 ± 0**
KOH-unextractable material[a], including	3 ± 1	3 ± 0	2 ± 1	2 ± 0	**6 ± 1**	**10 ± 0**	**50 ± 3**	**60 ± 2**	**32 ± 1**	**21 ± 1**	**5 ± 0**	**4 ± 0**	0 ± 0	0 ± 0
Cellulose-retained polymers[b]	3 ± 1	3 ± 0	2 ± 0	2 ± 1	**17 ± 2**	**35 ± 3**	w/o	w/o	**74 ± 2**	**56 ± 2**	3 ± 1	2 ± 1	1 ± 0	1 ± 0
Lignin-bound polymers[c]	8 ± 1	10 ± 1	**5 ± 0**	**7 ± 0**	**16 ± 2**	**22 ± 0**	**41 ± 7**	**25 ± 1**	18 ± 6	22 ± 2	12 ± 1	13 ± 1	1 ± 0	1 ± 0

[a]Obtained by TFA hydrolysis of the pellet remaining after AO and KOH treatments. [b]Obtained by TFA hydrolysis of polymers collected after dissolution of KOH-unextractable pellets with LiCl in *N*,*N*-dimethylacetamide (DMA) and cellulose degradation. [c]Obtained by TFA hydrolysis of pellets remaining after dissolution of KOH-unextractable pellets with LiCl in DMA and cellulose degradation.

Table III. *Yields of monosaccharides in fractions of TW and NW*

Data are means ± SE ($n = 3$ biological repeats). tr, Trace; w/o, without Glc, since Glc could have been derived from cellulose during the procedure used. Values with significant differences between NW and TW samples according to Student's *t* test ($P \leq 0.05$) are shown in boldface.

Fraction	Rha		Ara		Gal		Glc		Xyl(Man)		GalA		GlcA	
	NW	TW	NW	TW	NW	TW	NW	TW	NW	TW	NW	TW	NW	TW
							mg g^{-1} dry wt							
Buffer-extractable polymers	**0.1 ± 0.1**	**0.9 ± 0.1**	**0.1 ± 0.0**	**0.3 ± 0.2**	**0.4 ± 0.1**	**3.8 ± 0.4**	0.1 ± 0.1	0.2 ± 0.1	**0.3 ± 0.1**	**0.1 ± 0.0**	**0.2 ± 0.1**	**2.2 ± 0.3**	**0.0 ± 0.0**	**0.1 ± 0.01**
AO-extractable polymers	0.2 ± 0.0	0.2 ± 0.0	0.1 ± 0.0	0.1 ± 0.0	0.4 ± 0.3	0.8 ± 0.2	**0.7 ± 0.2**	**0.2 ± 0.1**	**1.4 ± 0.4**	**0.2 ± 0.2**	0.4 ± 0.1	0.4 ± 0.2	tr	tr
KOH-extractable polymers	4.5 ± 0.2	5.7 ± 0.9	**1.1 ± 0.1**	**2.7 ± 0.4**	**3.5 ± 0.6**	**18.6 ± 3.7**	**9.9 ± 0.8**	**8.5 ± 0.2**	**170.3 ± 19.9**	**72.2 ± 9.3**	18.1 ± 3.0	16.5 ± 2.1	**0.7 ± 0.2**	**1.8 ± 0.3**
KOH-unextractable material[a], including	1.3 ± 0.4	1.6 ± 0.4	0.8 ± 0.3	0.9 ± 0.4	**2.6 ± 0.4**	**5.8 ± 1.4**	**20.1 ± 3.4**	**34.2 ± 5.7**	11.9 ± 1.9	11.3 ± 2.7	2.4 ± 0.5	2.4 ± 0.7	0.1 ± 0.0	0.2 ± 0.1
Cellulose-retained polymers[b]	0.2 ± 0.0	0.3 ± 0.0	0.1 ± 0.0	0.1 ± 0.0	**1.4 ± 0.3**	**2.8 ± 0.4**	w/o	w/o	**5.4 ± 0.8**	**4.1 ± 0.1**	0.3 ± 0.1	0.2 ± 0.1	0.1 ± 0.0	0.1 ± 0.0
Lignin-bound polymers[c]	**0.7 ± 0.1**	**0.3 ± 0.0**	**0.4 ± 0.1**	**0.2 ± 0.0**	**1.4 ± 0.1**	**0.8 ± 0.0**	**3.8 ± 1.2**	**0.9 ± 0.0**	1.6 ± 0.6	0.8 ± 0.1	**1.2 ± 0.1**	**0.5 ± 0.1**	**0.1 ± 0.0**	**tr**

[a]Obtained by TFA hydrolysis of the pellet remaining after AO and KOH treatments. [b]Obtained by TFA hydrolysis of polymers collected after dissolution of KOH-unextractable pellets with LiCl in *N*,*N*-dimethylacetamide (DMA) and cellulose degradation. [c]Obtained by TFA hydrolysis of pellets remaining after dissolution of KOH-unextractable pellets with LiCl in DMA and cellulose degradation.

To investigate the nature of those galactans further, we structurally characterized them by PACE. For the analysis of AG-II, high-M_r subfractions of TW and NW (Fig. 3A) were adjusted to contain equal amounts of Ara and then hydrolyzed with two AG-II-specific enzymes. One was exo-β-1,3-galactanase, which hydrolyzes terminal β-(1→3)-Gal linkages but can bypass branching points liberating any β-(1→6)-galactan side chains with various DPs (Tsumuraya et al., 1990). The other was α-arabinofuranosidase, which removes terminal Ara residues (Takata et al., 2010). The resulting oligosaccharides were analyzed by gel electrophoresis. As shown in Figure 3D, the high-M_r subfractions of both NW and TW samples were susceptible to the enzymatic treatment, which released a ladder of oligosaccharides with DP ranging from 1 to 8. Some of the oligosaccharides comigrated with known standards (Tryfona et al., 2012) while others were of unknown identity. However, there were substantial differences in the abundance of the oligosaccharides released from the NW and TW samples. In particular, higher amounts of (Me)GlcA-Gal and (Me)GlcA-Gal_2, and lower amounts of β-(1→6)-Gal_4, were released by exo-β-(1→3)-galactanase from TW samples (Fig. 3D, red arrowheads). In addition, lower amounts of β-(1→6)-Gal_4, β-(1→6)-Gal_3, and an unidentified product, but higher amounts of (Me)GlcA-Gal (Fig. 3D, blue arrowheads), were released by a combination of α-arabinanase followed by exo-β-(1→3)-galactanase from TW samples. These results indicate that there are structural differences in buffer-soluble AG-II between NW and TW.

To investigate the nature of β-(1→4)-galactans in the high-M_r subfraction, NW and TW samples with equal total sugar contents were hydrolyzed with endo-β-(1→4)-galactanase, and the resulting oligosaccharides were analyzed by gel electrophoresis (Fig. 3E). The endo-β-(1→4)-galactanase hydrolysis resulted in a number of oligosaccharides with apparent DP ranging from 1 to 8, which comigrated with known standards. TW samples yielded considerably more of these fragments than NW samples (Fig. 3E, green arrowheads). Thus, β-(1→4)-galactan is far more abundant in TW (as TW samples have much higher buffer-extractable contents) than in NW. The galactanase used cuts unbranched β-(1→4)-galactan into products with DP 1 to 3 (Barton et al., 2006), and corresponding bands were the most intense. However, higher DP products were also detected, suggesting the presence of branching points or other obstacles for the enzyme's action. TW samples yielded more abundant and diverse products of this type, suggesting that β-(1→4)-galactan has a more complex structure in TW than in NW.

KOH-Extractable Polysaccharides

Some of the polymers in the major, KOH-extractable fractions of both TW and NW samples eluted in the greater than 500-kD region and constituted the highest molecular mass subfraction of all analyzed polysaccharides (Figs. 3–5). The rest eluted between 5 and 100 kD (Fig. 4A).

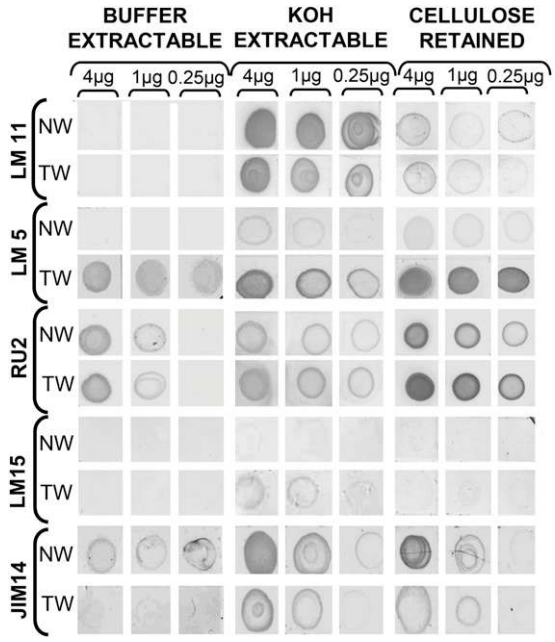

Figure 2. Immunodot analysis of cell wall polysaccharides in buffer-extractable, KOH-extractable, and cellulose-retained (obtained after cellulase treatment) fractions of NW and TW with antibodies recognizing (1→4)-β-xylan (LM11; McCartney et al., 2005), (1→4)-β-galactan (LM5; Jones et al.1997), RG-I backbone (RU2; Ralet et al., 2010), the XXXG motif of xyloglucan (LM15; Marcus et al., 2008), and an unknown epitope of AGP (JIM14; Knox et al., 1991). Total fractions (aliquots taken before gel filtration) were used for analysis. Values (4 μg, 1 μg, and 0.25 μg) on top of the membrane images indicate the amount of carbohydrates spotted on each vertical line of dots.

The sugar composition of the high-M_r subfraction was similar in TW and NW samples (Fig. 4B). In both cases, Xyl(Man) were the most abundant sugars. Accordingly, the LM11 antibody specific for β-(1→4)-xylan bound strongly to subfractions isolated from both NW and TW samples (Fig. 4D). To investigate whether mannans were present in the samples, the LM21 antibody that specifically binds β-(1→4)-mannan (Marcus et al., 2010) was used. Immunodot analysis confirmed the presence of β-(1→4)-mannan epitopes in this subfraction (Fig. 4D). In addition, it contained low amounts of Rha and Gal (more clearly detected in TW samples than in NW samples). The immunoblot analysis also revealed the presence of β-(1→4)-galactan and RG-I backbone, which is consistent with the presence of RG-I polymer in this subfraction. Signals from LM5 and RU2 antibodies were far stronger in TW than in NW samples, indicating that RG-I, and β-(1→4)-galactan epitopes, are more abundant in TW (Fig. 4D).

Xyl(Man) were also the most abundant sugars in the low-M_r subfraction, but Rha, Ara, Gal, Glc, and GalA were also detected (Fig. 4C). More Gal and less Xyl (Man) were found in TW than in NW. Immunoblot signals revealed the presence of β-(1→4)-xylan, β-(1→4)-mannan, β-(1→4)-galactan, and XG in this subfraction, of which β-(1→4)-galactan and XG were only detected in TW while β-(1→4)-xylan and β-(1→4)-mannan were detected in both TW and NW (Fig. 4).

The separation of polymers into two clear peaks (Fig. 4A), each of which contained Xyl(Man) and was labeled in immunodot analysis by LM11 and LM21 antibodies, suggested the presence of two populations of β-(1→4)-xylan and β-(1→4)-mannan molecules in the KOH-extractable fraction of both NW and TW. These populations might differ in the presence of some intermolecular interactions or linkages. Similarly, there were two populations of β-(1→4)-galactan, both of which were far more abundant in TW. XG was detected only in TW as an oligomer or low-M_r polysaccharide.

Cellulose-Retained Polymers

Polymers isolated from the alkali-unextractable pellets by dissolution with LiCl in DMA and subsequent cellulase treatment were separated by gel-filtration into two major subfractions with very distinct compositions (Fig. 5A). One was represented by a peak in the 50- to 200-kD molecular mass region and was more pronounced in TW samples, while the other eluted mainly in the less than 5-kD region and was less pronounced in TW samples than in NW samples. The latter had very similar monomeric sugar constitutions in NW and TW samples, with high Glc and Xyl contents, suggesting the presence of oligomeric fragments of xylan and probably contaminating products of cellulase digestion (Fig. 2), so it was not further examined. The higher molecular mass subfraction, in contrast, differed in composition between NW and TW (Fig. 5). The proportion of Gal, the major monomer, was considerably higher, while the proportion of Man, the second most abundant monomer and indicative of mannan, was lower in TW samples. The remaining monosaccharides (including Rha and GalA, indicative of RG-I) were present in similar proportions in both wood types (Fig. 2). Interestingly, Man was substantially more abundant than Xyl in the cellulose-retained fraction of both TW and NW, in sharp contrast to the 88:12 Xyl:Man ratio in the KOH-extractable fraction (Fig. 5).

The high-molecular-mass polysaccharides were further characterized by enzyme hydrolysis and PACE. Following the endo-(1→4)-galactanase treatment, oligosaccharides comigrating with Gal and β-(1→4)-galactan dimer and trimer were released from the TW samples. Very small amounts of β-(1→4)-galactooligosaccharides were detected in this fraction from NW (despite loading gels with the same amounts of total sugar as when analyzing TW samples), indicating that extremely little β-(1→4)-galactan is present in this fraction of NW, although it is the major polymer in the corresponding TW fraction (Fig. 5D, green arrowheads). To investigate whether the RG-I backbone was also present in this subfraction, the same amounts of TW and NW polymers were subjected to digestion by RG-I lyase, and the digestion products were analyzed by separating charged oligosaccharides on AMAC gels

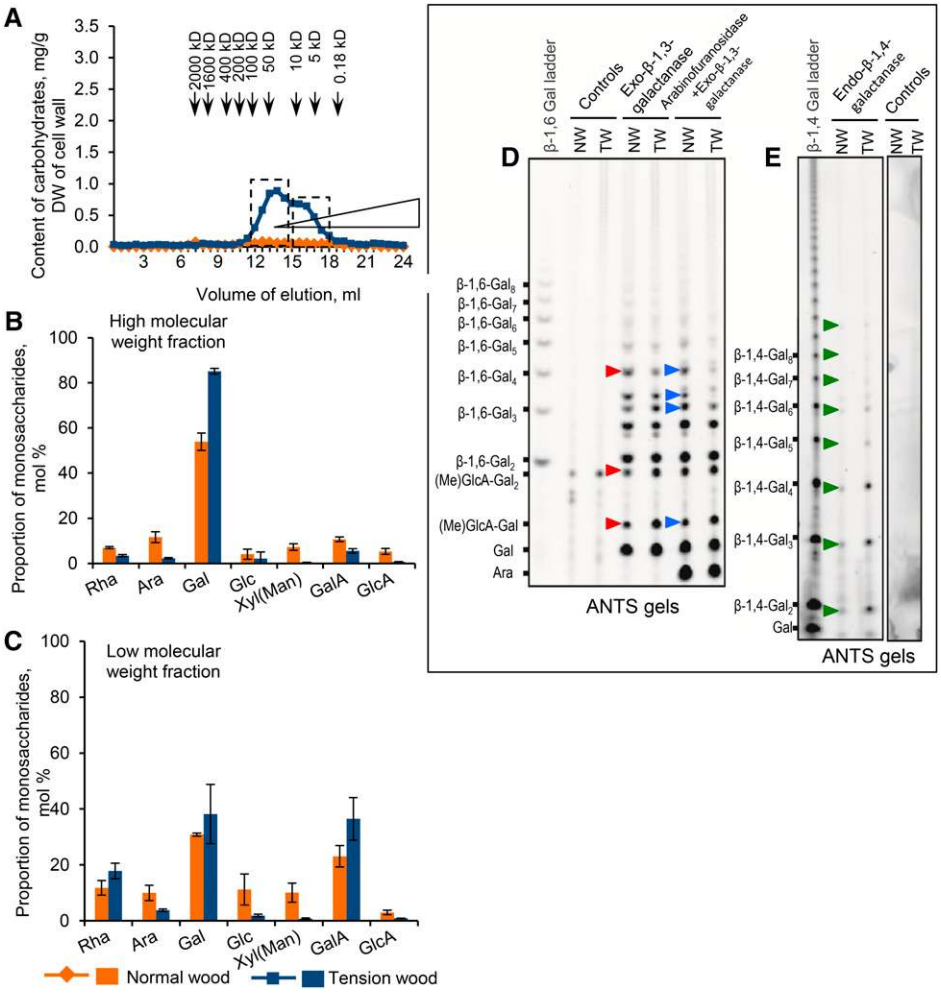

Figure 3. Analysis of two subfractions of buffer-extractable polysaccharides of NW and TW. A, Elution profile with designation of two subfractions. DW, Dry weight. B and C, Proportions of monosaccharides obtained after TFA hydrolysis of high- and low-molecular-weight fractions, respectively. Error bars show SE (n = 3 biological repeats). D and E, Oligosaccharide fragments obtained after enzymatic digestion and separation by PACE on 8-aminonaphthalene-l,3,6-trisulfonic acid (ANTS) gels. For the AG-II analysis, the high-molecular-mass subfractions of NW and TW were adjusted to equalize their total Ara contents and digested with exo-β-(1→3)-galactanase alone or in combination with arabinofuranosidase (D). For β-(1→4)-galactan analysis, the same samples were adjusted to equalize total sugar amounts and digested with endo-β-(1→4)-galactanase (E). Controls are the samples without enzymatic digestion to check for background signals. Bands with differing yields from NW and TW samples are marked by arrowheads: red, released by exo-β-(1→3)-galactanase; blue, released by α-arabinanase followed by exo-β-(1→3)-galactanase; and green, released by endo-β-(1→4)-galactanase.

(Tryfona et al., 2012). These treatments released and resolved a number of RG-I lyase products with various DPs. Due to the absence of appropriate standards, the released oligosaccharides could not be further characterized. However, comparison of the oligosaccharide profiles obtained from NW and TW samples shows that they differed in the abundance of some of the released oligosaccharides (Fig. 5D, orange arrowheads). This suggests that the RG-I branching pattern is modified in TW compared with NW. TW samples yielded considerably more of the analyzed subfraction than NW samples, suggesting that RG-I backbones are considerably more abundant in TW. AG-IIs were also analyzed by exo-β-(1→3)-galactanase hydrolysis and PACE. To allow direct comparison of NW and TW samples, they were adjusted to equalize their Ara contents before this analysis. Higher amounts of AG-II were present in TW relative to NW samples, according to differences in the abundance of Gal, (Me)GlcA-Gal, (Me)GlcA-Gal_2, and β-1,6-Gal_2 oligosaccharides (Fig. 5E, red arrowheads). This indicates that the TW subfraction contains more AG-II polysaccharides than the corresponding NW subfraction. Moreover, the proportion of these acidic oligosaccharides was higher in this subfraction of TW than in the buffer-soluble subfraction (compare Figs. 5 and 3), suggesting that there are structural differences between the AG-II in cellulose-retained and soluble polymer fractions of TW.

To obtain more structural information about the β-(1→4)-galactan that was found to be the most prominent of the high-M_r polymers in the cellulose-retained fraction of TW, a sample of these polymers was analyzed by NMR spectroscopy. In the anomeric region of the ^{1}H spectrum, the most intense signal arose from the H1 of β-D-Gal (4.63 ppm). Signals in the 4.72- to 5.25-ppm region could result from Man, Rha, and GalA residues. High-intensity signals in the aliphatic spectral region arose mainly from β-D-Gal. Signals at 4.63 (H1) and 4.16 (H4) ppm indicated that Gal is 1,4 linked. Signals at 1.24 and 1.32 ppm, respectively assigned to methyl groups of 2-Rha and 2,4-Rha, suggest that the relative proportions of branched and unbranched Rha were 47% and 53%. The ratio (2.71:0.45) of integral intensities of well-separated Gal signal (H4) and signals from the three protons of the methyl group of 2,4-Rha indicates that the average length of the β-(1→4)-Gal chains was approximately 18 monomers.

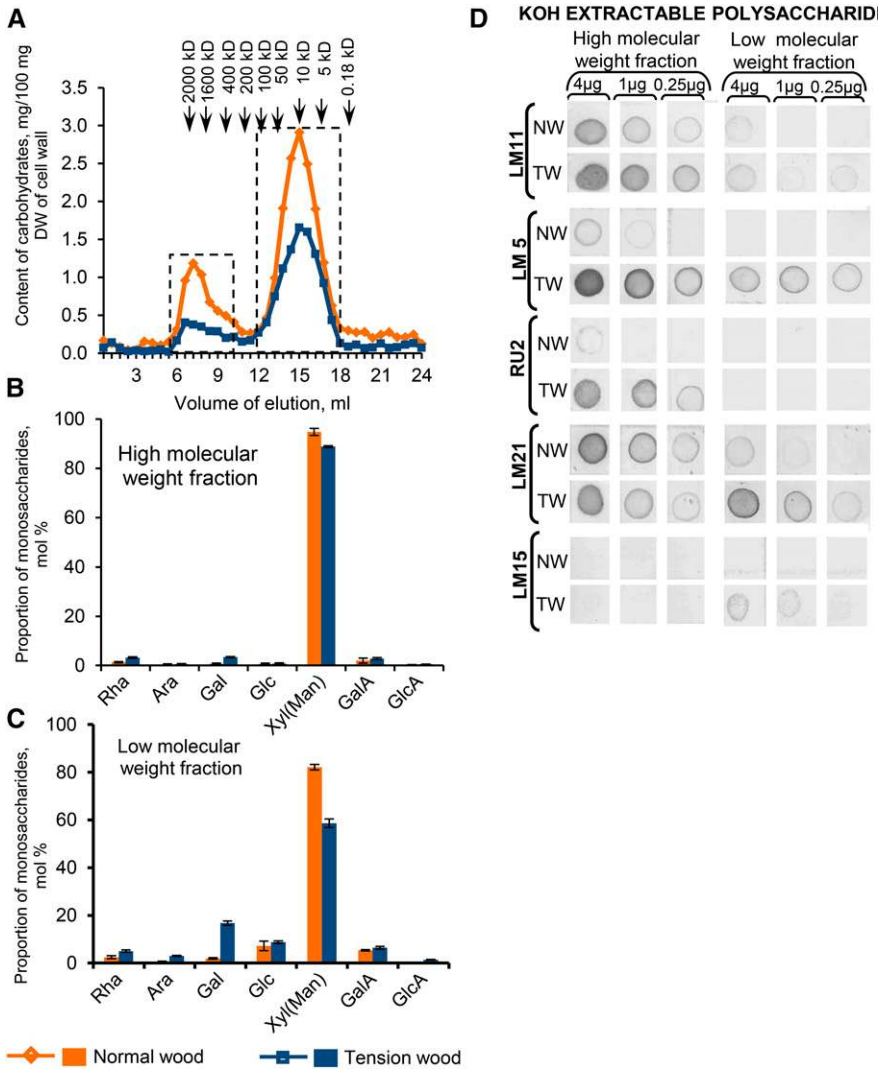

Figure 4. Analysis of two subfractions of KOH-extractable cell wall polysaccharides of NW and TW. A, Elution profile with designation of two subfractions. DW, Dry weight. B and C, Proportions of monosaccharides obtained after TFA hydrolysis of high- and low-molecular-weight fractions, respectively. Error bars show SE ($n = 3$ biological repeats). D, Immunodot analysis of the subfractions with antibodies recognizing (1→4)-β-xylan (LM11; McCartney et al., 2005), (1→4)-β-galactan (LM5; Jones et al., 1997), RG-I backbone (RU2; Ralet et al., 2010), (1→4)-β-mannan (LM21; Marcus et al., 2010), and the XXXG motif of xyloglucan (LM15; Marcus et al., 2008). Values (4 μg, 1 μg, and 0.25 μg) on top of the membranes indicate the amount of carbohydrates spotted on each vertical line of dots.

Immunocytochemical Localization of Polysaccharides in Wood Sections Identifies Polymers of the Compound Middle Lamella, S-Layers, and G-Layers

The polymers that were biochemically identified as differentially abundant in various fractions of TW and NW were localized in different cell wall layers by immunocytochemistry. Representative patterns of labeling are shown in Figure 6 and Supplemental Figure S2. The G-layers of TW fibers were heavily labeled with LM5 antibody, specific for β-(1→4)-galactans, while S-layers of both TW and NW were devoid of this labeling (Fig. 6, A and B). Signals from LM5 were also detected in the compound middle lamella in both TW and NW. A similar distribution was observed for RG-I backbone epitopes specifically recognized by the RU2 antibody (Fig. 6, C and D). A reciprocal label distribution was observed with LM11 antibody, which recognizes β-(1→4)-xylan, as it solely labeled S-layers in both TW and NW fibers (Fig. 6, E and F). LM15 revealed XG epitopes in the compound middle lamella, which were more abundant in TW than in NW, and some signals at the S-layer-G-layer boundary and innermost (developing) G-layers in TW fibers (Fig. 6, G and H). Attempts to immunolocalize AG-II by electron microscopy were not successful, although signals from the antibodies used were observed in the periplasm of ray parenchyma cells. Similar observations were reported by Lafarguette et al. (2004). We detected no labeling of fiber cell walls in either TW or NW samples by either the JIM14 antibody, recently classified by multivariate analysis as recognizing AG-II epitopes, designated AG-4, or M7 and M22 antibodies, classified as recognizing epitopes in RG-I and/or AG-II, designated RG-I/AG (Pattathil et al., 2010). LM21, which specifically binds to β-(1→4)-mannans, was the only antibody that bound both S-layers in TW and NW and G-layers in TW (Fig. 6, I and J). LM21 labeling was weaker in TW S-layers than in TW G-layers and NW S-layers. No labeling was detected in control experiments omitting primary antibodies.

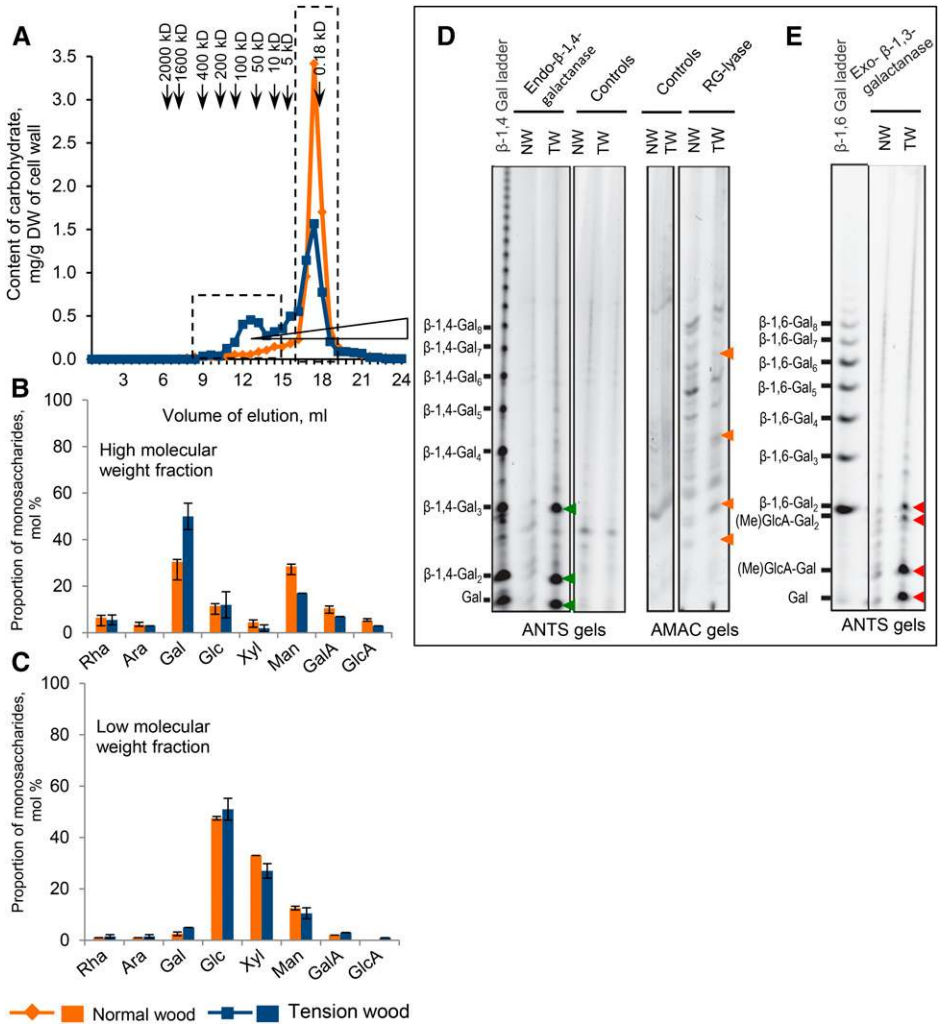

Figure 5. Analysis of two subfractions of cellulose-retained polymers from samples of NW and TW. A, Elution profile with designation of two subfractions. DW, Dry weight. B and C, Proportion of monosaccharides obtained after TFA hydrolysis of high- and low-molecular-weight fractions, respectively. Error bars show SE ($n = 3$ biological repeats). D and E, Oligosaccharide fragments obtained after enzymatic digestion and separation by PACE on ANTS or 2-aminoacridone (AMAC) gels. For the β-(1→4)-galactan, the high-molecular-mass subfractions of NW and TW were adjusted to equalize total sugar amounts and digested with endo-β-(1→4)-galactanase (D). For the RG-I backbone treatment experiments (Jensen et al., 2010), similar samples were digested with RG-I lyase (D). No standards were available for the RG-I fragments. For the AG-II analysis, the high-molecular-mass subfractions of NW and TW were adjusted to equalize amounts of total Ara and digested with exo-β-(1→3)-galactanase (E). Controls are the samples without enzymatic digestion to check for background signals. Bands with differing yields from NW and TW are marked by arrowheads: green, released with endo-β-(1→4)-galactanase; red, released with exo-β-(1→3)-galactanase; and orange, released with RG-I lyase.

In Situ Assays Reveal Higher β-1,4-Galactosidase Activity in TW Than in NW

In gelatinous fibers of flax, the β-(1→4)-galactan is modified by a cell wall GH35 β-galactosidase, which is essential for processing of the high-molecular-mass galactan and development of a highly crystalline cellulosic cell wall layer (Mikshina et al., 2009; Roach et al., 2011; Mokshina et al., 2012). Therefore, we investigated if the development of TW also involves β-1,4-galactosidase activity. Freshly prepared TW and NW sections were incubated with Gal-resorufin, and the release of resorufin by endogenous β-1,4-galactosidase activity was monitored in real time in situ, following Ibatullin et al. (2009) and Banasiak et al. (2014). β-1,4-Galactosidase signals were detected in developing NW and TW cell walls and were distinctly stronger in the latter (Fig. 7). In TW samples, the signals were most intense in the outer cell wall layers (perhaps the compound middle lamella) and G-layer. No signal was detected in control sections heated before the assay to denature proteins.

DISCUSSION

Key Differences in the Structure and Occurrence of Matrix Cell Wall Polysaccharides between TW and NW

The major cytological difference between TW and NW in aspen, as in many angiosperms, is the formation of a tertiary G-layer in TW fibers (Fig. 1). This layer lacks lignin and has very high cellulose contents, cellulose microfibrils oriented parallel to the fibers' longitudinal axes, large cellulose crystallites, high mezoporosity, and distinct matrix polysaccharides (for review, see Mellerowicz and Gorshkova, 2012). Further cytochemical and biochemical comparisons of matrix cell wall polysaccharides in aspen TW and NW revealed the following similarities and distinctions.

Xylan is by far the major matrix polymer in both TW and NW (Figs. 1 and 2; Tables I–III). However, the G-layer in aspen TW does not bind the anti-xylan antibody LM11, which heavily labels S-layers (Fig. 6). Previous assays with several antibodies recognizing secondary wall xylan (LM10, LM11, and AX1) indicate that xylan is also restricted to S-layers in gelatinous TW

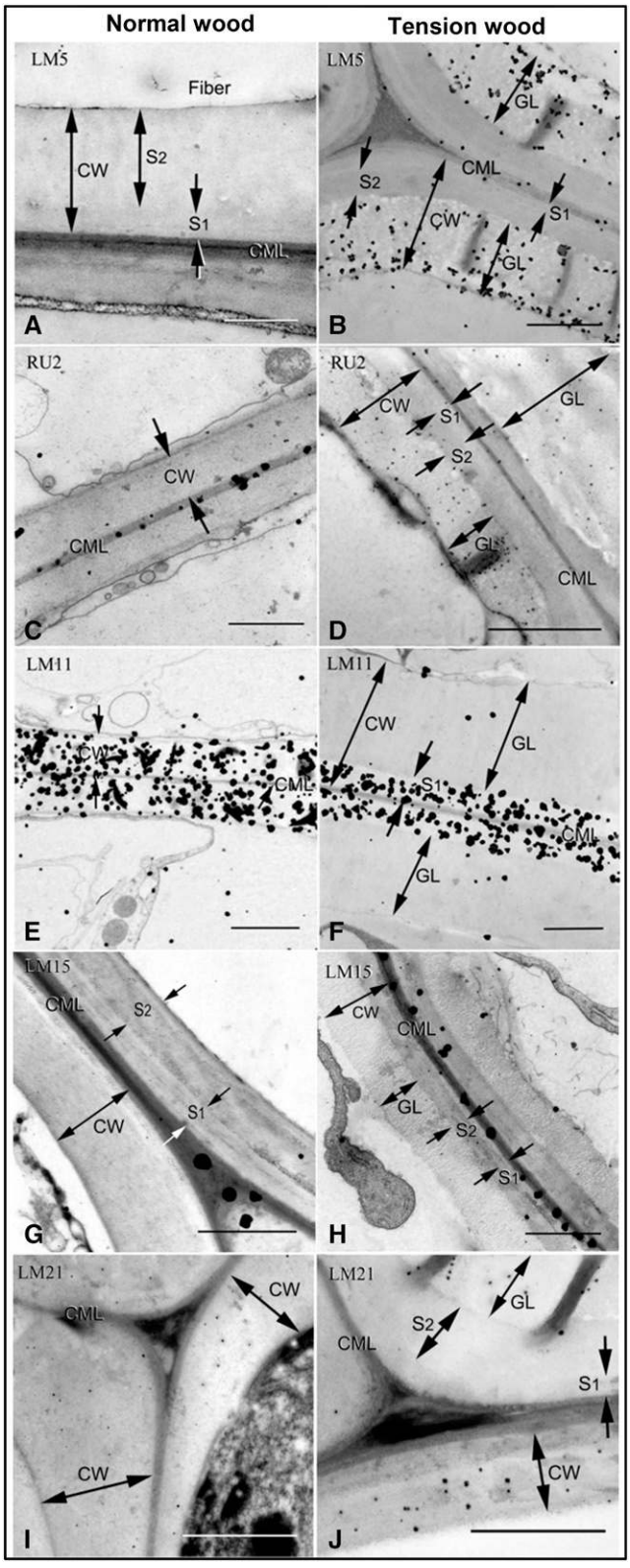

Figure 6. Immunolocalization of cell wall polysaccharides in fibers of NW (left) and TW (right) with LM5 antibody (A and B), RU2 antibody (C and D), LM11 antibody (E and F), LM15 antibody (G and H), and LM21 antibody (I and J). CML, Compound middle lamella; CW, cell wall; GL, G-layer, S1 and S2, secondary cell wall layers. Silver enhancement was applied for different times (2–5 min), leading to different sizes of particles. Bars = 1 μm.

of several species (Bowling and Vaughn, 2008, 2009; Decou et al., 2009). Sparse labeling of G-layers (relative to S-layers) by LM11 (with no LM10 labeling) in hybrid aspen has been reported (Kim and Daniel, 2012), but Nishikubo et al. (2007) detected no xylan in linkage analysis of isolated G-layers. Thus, exclusion of xylan from the G-layers appears to be the main cause of lower Xyl content in TW (Fig. 1). It also correlates with transcriptomic changes observed following TW induction in aspen, including the down-regulation of transcripts encoding UDP-Xyl synthase, Glycosyl Transferase8 (GT8) family members (GT8E, GT8F-1, GT8F-2 [similar to PARVUS], and GT8B-2 [similar to GLUCURONIC ACID SUBSTITUTION OF XYLAN1]), and GT47C, all of which are involved in xylan biosynthesis (Andersson-Gunnerås et al., 2006).

Various approaches, including wet chemistry and CCRC-M1 antibody labeling, have demonstrated the presence of XG, the characteristic polysaccharide of primary cell walls, which is absent or reduced in NW S-layers (Bourquin et al., 2002), in G-layers and S2/G boundaries of gelatinous fibers in *Populus* spp. and other species (Nishikubo et al., 2007; Bowling and Vaughn, 2008; Mellerowicz et al., 2008; Baba et al., 2009; Sandquist et al., 2010). Our LM15 labeling confirms its localization in the compound middle lamella, S2/G layer boundaries, and developing G-layers in aspen (Fig. 6). Sequential extraction and size-exclusion analyses presented here also show that XG with a low molecular mass (10 kD) is more abundant in KOH-extractable polymers of TW than in those of NW (Figs. 2 and 4). Only trace amounts of XG were present in the cellulose-retained polymer fraction in TW (Fig. 2).

The only matrix polymer deposited in both S-layers and G-layers is β-(1→4)-mannan (Fig. 6, I and J). Its presence in isolated G-layers is supported by sugar and linkage analysis (Furuya et al., 1970; Nishikubo et al., 2007). Labeling by LM21 was more prominent in G-layers, as reported previously (Kim and Daniel, 2012). However, Man and mannan contents were lower in TW than in NW (Fig. 1C; Hedenström et al., 2009), and transcripts encoding three GDP-Man-pyrophosphorylases, and the putative mannan synthase *Pt*GT2A, are reportedly correspondingly reduced (Andersson-Gunnerås et al., 2006). These findings indicate that mannan levels are reduced in S-layers of TW samples and that LM21 labels S-layers less intensely in TW than in NW (Fig. 6, I and J). Interestingly, mannan is one of the main polymers of the cellulose-retained fraction of both NW and TW, but it is more abundant in NW (Fig. 5). According to previous proposals, the polymer that interacts directly with cellulose in S-layers is mannan in conifers (Åkerholm and Salmén, 2001) and xylan in hardwoods (Salmén and Burgert, 2009), but

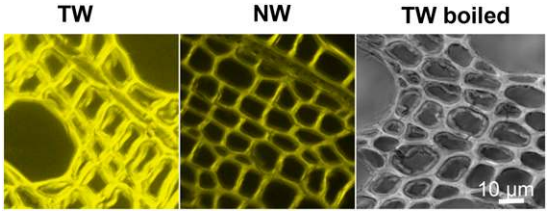

Figure 7. β-1,4-Galactosidase activity is present in cell walls of developing NW and TW and is highly increased in TW. Yellow coloration corresponds to the fluorescence channel signals from resorufin released by the action of β-1,4-galactosidase from the substrate. The control shown at right is the image of developing TW that was heated before the assay to denature proteins. No fluorescence signal was detected, and the image of the fluorescence channel was superimposed on the transmitted light channel to show the presence of TW tissue.

finding mannan in the cellulose-retained fraction (Fig. 5) suggests that it could also be intimately associated with cellulose in hardwood S-layers.

AG-II is a modular polysaccharide of variable structure decorating various AGPs (Tan et al., 2010). Since genes encoding AGPs similar to Arabidopsis *FASCICLIN-LIKE ARABINOGALACTAN-PROTEIN12* (*AtFLA12*) and *AtFLA11* are among the most strongly up-regulated genes following G-layer induction in several species (Lafarguette et al., 2004; Pilate et al., 2004; Paux et al., 2005; Andersson-Gunnerås et al., 2006; Roach and Deyholos, 2007), we predicted that specific forms of AG-II would be more abundant in TW compared with NW. An 8-fold increase of the buffer-soluble fraction in TW (Table I), which is expected to contain most AGPs due to their high water solubility and proposed periplasmic location (Lamport and Várnai, 2013), and structural differences between buffer-soluble AG-II of TW and NW (Fig. 3) confirmed that specific AGPs are up-regulated in TW. These AGPs were not recognized by JIM14, which labeled AG-II in all analyzed fractions more strongly in NW than TW and KOH-extractable polymers most strongly (Fig. 2). Thus, these JIM14 signals in AG-II probably did not correspond to FLA11- and FLA12-like AGPs. In addition to high abundance in the buffer-soluble fraction, AG-II has been identified as one of the main compounds of cellulose-retained high-M_r polymers (Fig. 5). Interestingly, this fraction of TW contained significantly more exo-β-(1→3)-galactanase-susceptible AG-II, relative to Ara, than the corresponding NW fraction, suggesting that β-(1→3)-galactan specifically expands in TW. Moreover, both buffer-soluble and cellulose-retained AG-II polymers of TW were more acidic than those of NW (Figs. 3D and 5E). Acidic forms of AGP could play more than a structural role in TW. GlcA of AG-II may be involved in the stoichiometric binding of Ca^{2+} (Lamport and Várnai, 2013), which plays key roles in plant signaling pathways (Kudla et al., 2010). Thus, our data imply that Ca^{2+} associated with special acidic AG-II may participate in TW development.

Our data also clearly show that higher abundance of RG-I backbone and long β-(1→4)-galactan chains are the main biochemical features distinguishing TW from NW (Figs. 2–5; Tables II and III). Higher proportions of Gal have been detected in TW than in NW of several species (Meier, 1962; Kuo and Timell, 1969; Furuya et al., 1970; Ruel and Barnoud, 1978; Mizrachi et al., 2014), and β-(1→4)-galactan has been detected in G-layers of aspen (Arend, 2008). However, β-(1→4)-galactan has not been shown previously to cooccur with RG-I in TW. We detected RG-I backbone and β-(1→4)-galactan signals from RU2 and LM5 antibodies, respectively, in the compound middle lamella and G-layer (Fig. 6). We also detected RG-I backbone and β-(1→4)-galactan in all polysaccharide fractions of TW (Figs. 2 and 5), including polymers retained in cell walls so tightly that they can be extracted only after dissolution of cellulose microfibrils. In lignified cell walls, a polysaccharide may remain unextractable by strong alkali if it is linked to lignin, but as there is virtually no lignin in G-layers (Love et al., 1994; Gorshkova et al., 2000; Kaku et al., 2009), the RG-I with β-(1→4)-galactan, immunolocalized in G-layers, could only remain unextracted if trapped between cellulose microfibrils.

Differences and Similarities between Flax and Aspen Gelatinous Fibers

As in flax fibers, RG-I backbone is present, together with β-(1→4)-galactan chains, in the polymers retained in TW by cellulose microfibrils. The structure of the TW RG-I coextracting with β-(1→4)-galactan resembles that of flax phloem fibers: according to the NMR analysis presented here and by Mikshina et al. (2012), the degree of RG-I backbone substitution is 50% in aspen and 30% in flax phloem, and the average length of β-(1→4)-Gal chains in these species is 18 and 14, respectively. Although we have not demonstrated the linkage between Rha and Gal in aspen, it has been fully resolved in flax (Mikshina et al., 2012, 2015). Flax fiber RG-I molecules can form water-soluble complexes having β-(1→4)-galactan chains in the center and acidic RG-I backbones at the periphery (Mikshina et al., 2015). Structural similarities suggest that the aspen TW counterpart also has such ability. Acidic AG-II, detected in the cellulose-retained fraction of aspen TW, has not been characterized to date in flax fibers. However, strong up-regulation of FLA11- and FLA12-like AGPs during flax fiber development (Roach and Deyholos, 2007) suggests that this form of AG-II is also present in flax. The relationship between AG-II and RG-I, both of which are potential sources of carboxylic acid residues observed by dynamic Fourier transform infrared spectroscopy in aspen TW (Olsson et al., 2011), remains to be determined.

In flax, mature G-layers form from initially deposited G-layers, called Gn, which can be clearly distinguished in electron micrographs (Gorshkova et al., 2004, 2010). The maturation involves the postdeposition modification of nascent RG-I galactan by the galactosidase *Lu*BGAL1 (Mikshina et al., 2009; Roach et al., 2011;

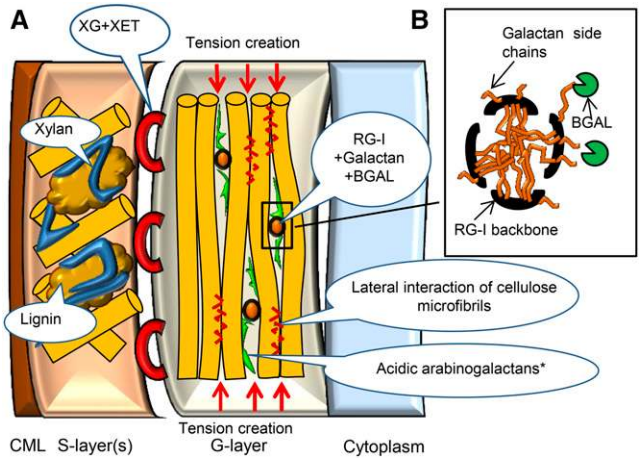

Figure 8. A, Scheme of the main components in S-layers and G-layers of fibers in TW. In S-layers, cellulose microfibrils are oriented helicoidally with alternating MFA between layers; in thick G-layers, the orientation of all cellulose microfibrils is close to axial. XG+XET, XG and xyloglucan endotransglycosylase, which acts to staple S-layers and G-layers (Mellerowicz et al., 2008; Hayashi et al., 2010). Cellulose microfibrils in S-layers are separated by xylan and lignin and have poor chances to interact laterally; in highly cellulosic G-layers, microfibrils tend to interact laterally, thereby increasing crystallinity. RG-I+Galactan, RG-I and β-(1→4)-galactan trapped between laterally interacting G-layer cellulose microfibrils, creating tension in them. Galactan chains are modified in muro by a specific galactosidase (BGAL), making the polymer more compact and providing conditions for the lateral interaction of cellulose microfibrils (not shown). CML, Compound middle lamellae. B, Possible spatial structure of the RG-I and galactan (Mikshina et al., 2015): β-(1→4)-galactan side chains (galactan) attached to RG-I backbone. Molecules of RG-I are associated due to β-(1→4)-galactan chain interaction. Note that the backbone is located at the surface of such associated molecules.

Mokshina et al., 2012) and is essential for the flax stem's mechanical properties (Roach et al., 2011). The Gn structure is not pronounced in TW fibers, but many studies have detected an inner G-layer with different properties from the rest (Joseleau et al., 2004; Lafarguette et al., 2004; Gierlinger and Schwanninger, 2006). Moreover, we detected high β-galactosidase activity in developing TW fibers (Fig. 7), and a flax-specific galactosidase epitope has been detected in the G-layer of aspen TW (Mokshina et al., 2012), strongly suggesting the involvement of a homologous galactosidase in pectic β-(1→4)-galactan processing in TW.

The key difference in cell wall organization between gelatinous phloic fibers of flax and gelatinous xylary fibers of aspen concerns the degree of S-layer development. The flax S-layer is difficult to discern even in electron micrographs (Andème-Onzighi et al., 2000; Salnikov et al., 2008) but can be revealed by labeling with xylan-specific antibodies (Gorshkova et al., 2010). Thus, both types of gelatinous fibers have the same general type of cell wall architecture, with primary, secondary, and tertiary walls. Aspen TW fibers, as in other tree species, always have at least one well-developed S-layer (Fagerstedt et al., 2014) characterized by the presence of xylan and a helicoidal orientation of cellulose microfibrils with high cellulose microfibril angles (Clair et al., 2011; Rüggeberg et al., 2013). A xylan layer with nearly transverse cellulose orientation is probably required for its resistance to radial compression, which is poor in the G-layer with axial cellulose orientation. In herbaceous plants, the mechanical forces acting on developing phloem fibers in the radial direction (and, hence, the need for S-layers) may be weaker than in woody plants.

Thus, although flax and aspen are sufficiently closely related to belong to the same order (Malpighiales), they develop gelatinous fibers in different tissues and of different origin (in primary phloem initiated from the procambium and in secondary xylem produced by the vascular cambium, respectively). The structural similarities of these fibers suggest that other contractile cell walls with G-layers may also have similar structures and properties.

Implications of the Findings for the Entrapment-Based TW Contraction Hypothesis

TW plays a key physiological role in maintaining stems and branches with secondary growth in appropriate positions by generating tensional longitudinal stress. Characteristic contractile properties of TW with gelatinous fibers are known to originate from the G-layers (Clair and Thibaut, 2001; Yamamoto et al., 2005; Clair et al., 2006; Fang et al., 2008) that are firmly attached to S-layers in their native state (Clair et al., 2005), possibly through XG cross links (Nishikubo et al., 2007; Bowling and Vaughn, 2008; Sandquist et al., 2010). The G-layers were long assumed to consist almost entirely of cellulose (Norberg and Meier, 1966). Consequently, hypotheses regarding the origin of tension were based on the arrangements of cellulose microfibrils (Burgert and Fratzl, 2009). All microfibrils in thick G-layers lie almost parallel to each other and the longitudinal cell axis, in sharp contrast to the helicoidal arrangement of microfibrils in secondary cell wall layers (Rüggeberg et al., 2013; Fagerstedt et al., 2014). The difference in microfibril orientation provides the basis for pine (*Pinus* spp.) cone opening and wheat (*Triticum aestivum*) awn movement mechanisms (Burgert and Fratzl, 2009) and may be involved in the creation of tension in TW (Goswami et al., 2008). However, this mechanism is highly dependent on air humidity, and the movement is reversible, which is not the case in TW. Thus, additional factors must influence tension creation involving G-layers.

Rediscovery of the significant content of matrix polysaccharides in the G-layer (for review, see Mellerowicz and Gorshkova, 2012; Fagerstedt et al., 2014) increased attention to their possible role in tension generation (Fournier et al., 2014). Recent evidence shows that cellulose crystallites of the G-layers have larger lattice spacing than corresponding crystallites of the S-layers in NW, and this difference appears as the G-layer is deposited (Clair et al., 2011). The spacing is reduced as

the tension stress is released, and its reduction corresponds exactly to the macroscopic strain at the stem surface, indicating that cellulose fibrils are under tension in TW (Clair et al., 2006). We previously suggested that the tension could arise during microfibril lateral interaction with the entrapment of matrix polysaccharides (Mellerowicz et al., 2008; Mellerowicz and Gorshkova, 2012). With low matrix polysaccharide contents and no lignin, microfibril lateral contacts are frequent in the G-layer, leading to the formation of macrofibrils and explaining its high crystallinity (Müller et al., 2006; Yamamoto et al., 2009). However, the entrapment of polysaccharides between cellulose microfibrils would limit their interaction and force them to bend around these polymers, thereby increasing the longitudinal lattice distance, stretching the microfibrils and creating tension in them (Mellerowicz et al., 2008; Mellerowicz and Gorshkova, 2012).

This work identified polymers trapped within cellulose fibrils in TW of hybrid aspen as RG-I with β-(1→4)-galactan accompanied by a specific acidic form of AG-II. Conditions for the lateral interaction of cellulose microfibrils in TW may be provided in muro by trimming of the deposited galactans by fiber-specific galactosidases (Roach et al., 2011; Mokshina et al., 2012; Fig. 7). A gelatinous fiber model consistent with these new data is presented in Figure 8. RG-I with β-(1→4)-galactan is thought to form water-soluble supramolecular structures with low affinity to cellulose (Mikshina et al., 2015). The high hygroscopicity of RG-I (and possibly acidic AG-II) would retain water in the G-layer (Schreiber et al., 2010), accounting for the gel-like properties of these layers and their collapse during TW drying (Clair et al., 2006, 2008). Pockets containing these hydrated polymers could also explain the characteristically high mesoporosity of G-layers (Clair et al., 2008; Chang et al., 2009, 2015). Mesopores of various sizes (2–60 nm) and shapes (ink bottle and slit like) reportedly form during G-layer deposition (Chang et al., 2015), correlating with tensional stress development (Clair et al., 2011). Thus, the hydrated galactans identified in this study as cellulose-retained polymers could provide the contractile driving force in TW G-layers.

MATERIALS AND METHODS

Plant Material

Rooted cuttings of hybrid aspen (*Populus tremula* × *Populus tremuloides*), clone T89, were grown in a greenhouse at 20°C and 60% relative humidity with an 18-h photoperiod and supplementary lighting (Powerstar HQI-BT 400 W/D; Osram) switched on when the incoming light fell below 20 W m^{-2} during the photoperiod. Plants were watered daily and fertilized with a complete nutrient solution (SuperbaS; Supra HydrO) once per week. To induce TW, five 1-month-old plants were tilted at 45° from vertical with their basal stem parts secured to tilted stakes, at approximately 1 m from the base, and they were grown in this position for approximately 6 weeks. Control trees were grown in an upright position with their stems secured to vertical stakes. Approximately 1 m of the basal part of the stem from both tilted and upright trees was harvested, frozen in liquid nitrogen, and kept at −20°C until analysis. TW produced by the tilted trees, and NW produced by the upright trees, were dissected from stem segments and freeze dried, ground in a ZM 200 centrifugal mill (Retsch) at 14,000 rpm, and in each case the resulting powder was passed through a sieve with 0.5-mm mesh.

Cell Wall Isolation and Fractionation

Portions of the powdered TW and NW samples (1 g for each replicate) were homogenized on ice in 30 mL of 50 mM KH_2PO_4-NaOH buffer, pH 7. After centrifugation of each homogenate (8,000*g*, 25 min), the supernatant was filtered and incubated for 15 min in a boiling water bath to inactivate endogenous enzymes. The supernatant was then cooled, ethanol was added to 80% (v/v), and the mixture was incubated overnight at 4°C to precipitate the buffer-extractable polysaccharides. The resulting pellet was washed three times with 80% (v/v) ethanol and once with 80% (v/v) acetone and then dried.

Cell wall material from each pellet obtained after homogenization was isolated according to Talmage et al. (1973). Briefly, it was sequentially washed with water (3×), 80% (v/v) ethanol, acetone (overnight, 4°C), water (3×), and 50 mM KH_2PO_4-NaOH buffer (pH 7; 2×), digested overnight with 2 mg mL^{-1} glucoamylase supplied by Siekagaki Kogyo, washed with the same phosphate buffer, water (3×), and acetone, and then dried.

Cell wall polymers were extracted sequentially by 1% (w/v) AO (pH 5, boiling water bath, 1 h) and, after washing with water, by 4 M KOH with 3% H_3BO_4 (2 h). The KOH fractions were neutralized by adding acetic acid to pH 7. Fractions extracted by AO and alkali were desalted by passage through a Sephadex G-25 column (19 × 400 mm) and dried.

The residue remaining after AO and KOH treatment was washed by water and dried. A 2-mg portion was hydrolyzed by incubation with 2 M TFA at 120°C for 1 h to determine its sugar content by monosaccharide analysis. The rest of the pellet was used to isolate matrix polysaccharides in polymeric form, following Gurjanov et al. (2008). Briefly, it was dissolved in 8% (w/v) LiCl in DMA, and cellulose was precipitated by water and degraded by incubation with 1% (v/v) Cellusoft-L cellulase (Novo Nordisk Bioindustrie; 750 EGU/G) in 10 mM NaOAc buffer, pH 5.2, at 33°C overnight. Supernatants obtained after dissolution with LiCl in DMA and cellulose degradation were concentrated by partial lyophyllization, separated from salts and low-M_r products of cellulose digestion by passage through a Sephadex G-25 column (19 × 400 mm), combined, and dried. The resulting fraction was designated the cellulose-retained polymers.

The pellet remaining after partial removal of KOH-unextractable matrix polymers and cellulose digestion was washed by water, dried, hydrolyzed by 2 M TFA, and subjected to monosaccharide analysis (to obtain lignin-bound polymers). The difference between the pellet dry mass and total monosaccharide yield was designated the lignin content. The fractionation procedure is summarized in Supplemental Figure S1.

Cellulose content was calculated by subtracting the yields of all obtained fractions (buffer-extractable, AO-extractable, KOH-extractable, and KOH-unextractable polymers and lignin) from the dry mass of the initial sample.

Gel Filtration by HPLC

The obtained fractions of matrix polysaccharides were dissolved in 0.2 M Na_2HPO_4 with 0.05% (w/v) NaN_3, pH 6.8. Aliquots were taken for sugar content determination by the phenol-sulfuric acid method (Dubois at al., 1956), for monosaccharide analysis, and for immunodot analysis of total fractions. Portions (500–1,000 μg) of the obtained fractions were size-fractionated in the same buffer by an HPLC system (Gilson) equipped with combined G5000PW and G4000PW TSKgel columns (Tosoh Bioscience). Calibration was performed using dextran (2,000 kD; Sigma), pullulan standards with molecular masses of 1,600, 400, 200, 100, 50, 10, and 5 kD (Waters), and Gal (0.18 kD; Merck). To obtain elution profiles after gel filtration, 0.6-mL probes were collected and total sugars were quantified in each probe by the phenol-sulfuric acid method (Dubois et al., 1956) using Glc (Merck) as a standard. The presented elution profiles are means obtained from three independent biological replicates based on the carbohydrate contents of the probes and total amounts of sugar in the fractions.

According to the two major peaks in the elution profiles, buffer-soluble, KOH-extractable, and cellulose-retained polymers were each subdivided into two subfractions. Corresponding probes were combined, desalted by passage through a Sephadex G-25 column (15 × 50 mm), and concentrated using a vacuum evaporator. Portions of these preparations were used for monosaccharide determination and (when applied) immunochemical characterization or enzymatic hydrolysis with PACE.

Monosaccharide Analysis

Samples for monosaccharide analysis were dried, hydrolyzed with 2 M TFA at 120°C for 1 h, dried to remove TFA, dissolved in water, and analyzed by high-performance anion-exchange chromatography using a DX-500 instrument equipped with a 4- × 250-mm CarboPac PA-1 column and a pulsed amperometric detector (all from Dionex). The column temperature was 30°C, and the mobile phase (pumped at 1 mL min^{-1}) consisted of 100% B (0–20 min), 90% B (20–21 min), 50% B (22–41 min), 0% B (42–55 min), and finally 100% B (56–85 min), where B was 15 mM NaOH and the other solvent (A) was 100 mM NaOH in 1 M sodium acetate. In some additional experiments, Xyl and Man were separated by isocratic elution with 1.8 mM NaOH buffer. The results were analyzed using PeakNet software according to the calibrations obtained for monosaccharide standards treated in advance with 2 M TFA at 120°C for 1 h. Three independent biological replicates and two analytical replicates of NW and TW samples were analyzed.

Immunodot Analysis

Total fractions or subfractions containing 4, 1, and 0.25 μg of sugar (1–3 μL) were applied to nitrocellulose membranes (0.2 m; Sigma). Membranes were air dried for 30 min, washed for 5 min in PBST (phosphate-buffered saline with 0.05% [v/v] Triton X-100), blocked for 1 h with phosphate-buffered saline containing 3% (w/v) nonfat dry milk, and then incubated for 40 min with primary monoclonal antibody. The monoclonal antibodies used were LM5 (Jones et al., 1997), LM11 (McCartney et al., 2005), LM15 (Marcus et al., 2008), LM21 (Marcus et al., 2010), JIM14 (Knox et al., 1991), and RU2 (Ralet et al., 2010), all raised in rat except RU2 (mouse, hybridoma supernatant). They are specific for β-(1→4)-galactan, β-(1→4)-xylan, the XXXG motif of XG, β-(1→4)-mannan, an unknown epitope of AGP, and RG-I backbone, respectively. The antibodies were kindly provided by Paul Knox (LM5, LM11, LM15, LM21, and JIM14) and Dr. Fabienne Guillon (RU2). LM5, LM11, LM15, LM21, and JIM14 were applied at 1:30 dilution, and RU2 at 1:10 dilution, in PBST. After incubation with primary antibodies, membranes were washed three times for 10 min with PBST and then incubated with secondary biotinylated antibodies (Sigma; anti-rat to detect LM5, LM15, LM11, LM21, and JIM14 primary antibodies and anti-mouse to detect RU21) for 40 min. The membranes were washed again three times in PBST for 10 min, incubated for 30 min in streptavidin conjugated with alkaline phosphatase diluted 1:3,000, and developed using a nitroblue tetrazolium/5-bromo-4-chloro-3-indolyl phosphate kit (Silex). Potato (*Solanum tuberosum*) galactan and RG-I, arabinoxylan from wheat (*Triticum aestivum*) flour, and XG from tamarind (*Tamarindus indica*) seeds (all supplied by Megazyme) were used as positive controls.

Enzymatic Hydrolysis and PACE

For β-(1→4)-galactan analysis, subfractions of interest with equal amounts of total sugars were digested by incubation with endo-β-(1→4)-galactanase in 10 mM ammonium acetate, pH 6, at 37°C for 24 h. β-(1→4)-Galactan standards were prepared from lupin (*Lupinus albus*) seed pectic galactan (Megazyme) by endo-β-(1→4)-galactanase hydrolysis. For treatment with RG-I lyase prepared from *Aspergillus aculeatus* (Jensen et al., 2010), samples adjusted to equal amounts of total sugar were dissolved in 500 μL of 0.05 M Tris-HCl solution, pH 8, containing 2 mM $CaCl_2$ and incubated at 21°C for 24 h. For AG-II analysis, samples were adjusted to equal amounts of total Ara and hydrolyzed by arabinogalactan-specific enzymes as described by Tryfona et al. (2012). Carbohydrates were derivatized, electrophoretically separated, and subjected to PACE gel scanning and quantification as described by Goubet et al. (2002, 2009). Neutral fragments were separated on ANTS gels and acidic fragments on AMAC gels. The identity of digestion products was established by mass spectrometry in a previous study (Tryfona et al., 2012). Control experiments without substrates or enzymes were performed under the same conditions to detect nonspecific compounds potentially present in the enzyme preparations, polysaccharides/cell walls, or labeling reagents.

Transmission Electron Microscopy and Immunocytochemistry

Segments (approximately 5 mm × 5 mm × 15 mm in tangential, radial, and longitudinal directions, respectively) containing developing TW and NW were cut from the stem of tilted (Fig. 1) and upright trees, put immediately in 4% (w/v) paraformaldehyde + 0.5% (w/v) glutaraldehyde in 0.05 M sodium-phosphate buffer (pH 7.4), cut into 2-mm × 3-mm × 5-mm pieces, and infiltrated under vacuum for 5 min. Then, the samples were cut into smaller (1.5 mm × 1.5 mm × 2.5 mm) pieces, left in fresh portions of the same buffer for 3 h at room temperature, and postfixed with 0.5% (w/v) OsO_4 in 0.1 M sodium-phosphate buffer (pH 7.4) for 4 h. After dehydration, the samples were embedded in LR White resin (Medium Grade Acrylic Resin; Ted Pella; catalog no. 18181). Ultrathin sections were cut with a diamond knife and LKB Ultracut III ultramicrotome and then mounted on formvar-coated 100-mesh nickel grids. For immunolocalization, thin sections on nickel grids were blocked (15 min, room temperature, in a high-humidity chamber) in 0.02 M Tris-buffered saline, pH 7.5, and 0.1% (v/v) Tween 20 plus 5% (v/v) goat serum (Sigma; 5-2007) and incubated for 1 to 1.5 h at room temperature with LM5, LM11, LM21, or RU2 primary antibody (for information on antibodies, see above). LM5, LM11, and LM21 antibodies were used at 1:200 dilution in 0.02 M Tris-buffered saline, pH 7.5, and 0.1% (v/v) Tween 20 plus 5% (v/v) normal goat serum, while RU2 antibody was used without dilution. After incubation with each antibody, the samples were washed three times in 0.02 M Tris buffer, pH 8.2, with 0.02% (w/v) azide, incubated in secondary antibody (1:50 goat anti-rat for LM5 and LM11 and 1:50 goat anti-mouse for RU2) coupled in both cases to 5-nm colloidal gold (Amersham Pharmacia Biotech) in Tris buffer plus 0.06% (v/v) bovine serum albumin for 1 to 1.5 h at room temperature, then washed in Tris buffer and water. A BBInternational Silver Enhancing Kit (Ted Pella) was used to enhance signals of gold particles conjugated with secondary antibody. The solution was applied for 2 to 5 min (Hainfeld and Powell, 2000). Sections were stained for 20 min with 2% (w/v) aqueous uranyl acetate and then for 2 min with lead citrate at room temperature (Reynolds, 1963, Bozzola and Russell, 1999). Primary antibodies were omitted in control experiments. Sections were observed and photographed using a 1200 EX transmission electron microscope (JEOL) operating at 80 kV.

NMR Spectroscopy

Polymers obtained after cellulose dissolution were dissolved in 99.9 atom% heavy water (Ferak), dried, and then redissolved in 99.994 atom% heavy water (Aldrich). ^1H spectra were recorded at 303 K using a Bruker AVANCE III NMR spectrometer operating at 600 MHz. The acquired data were processed and analyzed using Topspin 2.1 software (Bruker).

In Situ β-Galactosidase Activity

The substrate for β-1,4-galactosidase, resorufinyl-4-*O*-(β-D-galactopyranoside), synthesized as described by Ibatullin et al. (2009), was a gift from Dr. Harry Brumer. Free-hand TW and NW sections were placed in assay buffer containing 47 mM resorufinyl-4-*O*-(β-D-galactopyranoside) and 25 mM MES at pH 6.5, and the evolution of the fluorescent signal from resorufin was monitored by time-lapse confocal microscopy during 80 min, using an LSM 510 instrument (Carl Zeiss). The presented micrographs were taken when the signal plateaued, after 20 min. The argon-krypton laser line at 568-nm excitation and over 570-nm emission was used. Signals from the transmitted light channel and fluorescence channels were recorded separately. Control sections were heated at 95°C in the MES buffer for 30 min prior to incubation with the substrate, using the same scanning conditions as for experimental sections.

Supplemental Data

The following supplemental materials are available.

Supplemental Figure S1. Scheme of the sequential extraction of cell walls.

Supplemental Figure S2. Immunolocalization of cell wall polysaccharides in fibers of normal wood and tension wood.

ACKNOWLEDGMENTS

We thank Dr. Harry Brumer (University of British Columbia) for Gal-β-resorufin and both Dr. Paul Knox (University of Leeds) and Dr. Fabienne Guillon (Institut National de la Recherche Agronomique) for the antibodies.

Received May 7, 2015; accepted September 12, 2015; published September 16, 2015.

LITERATURE CITED

Åkerholm M, Salmén L (2001) Interactions between wood polymers studied by dynamic FT-IR spectroscopy. Polymer (Guildf) **42:** 963–969

Andème-Onzighi C, Girault R, His I, Morvan C, Driouich A (2000) Immunocytochemical characterization of early-developing flax fibre cell walls. Protoplasma **213:** 235–245

Andersson-Gunneràs S, Mellerowicz EJ, Love J, Segerman B, Ohmiya Y, Coutinho PM, Nilsson P, Henrissat B, Moritz T, Sundberg B (2006) Biosynthesis of cellulose-enriched tension wood in *Populus*: global analysis of transcripts and metabolites identifies biochemical and developmental regulators in secondary wall biosynthesis. Plant J **45:** 144–165

Arend M (2008) Immunolocalization of (1,4)-beta-galactan in tension wood fibers of poplar. Tree Physiol **28:** 1263–1267

Baba K, Park YW, Kaku T, Kaida R, Takeuchi M, Yoshida M, Hosoo Y, Ojio Y, Okuyama T, Taniguchi T, et al (2009) Xyloglucan for generating tensile stress to bend tree stem. Mol Plant **2:** 893–903

Banasiak A, Ibatullin FM, Brumer H, Mellerowicz EJ (2014) Glycoside hydrolase activities in cell walls of sclerenchyma cells in the inflorescence stems of *Arabidopsis thaliana* visualized *in situ*. Plants **3:** 513–525

Barton CJ, Tailford LE, Welchman H, Zhang Z, Gilbert HJ, Dupree P, Goubet F (2006) Enzymatic fingerprinting of Arabidopsis pectic polysaccharides using polysaccharide analysis by carbohydrate gel electrophoresis (PACE). Planta **224:** 163–174

Bourquin V, Nishikubo N, Abe H, Brumer H, Denman S, Eklund M, Christiernin M, Teeri TT, Sundberg B, Mellerowicz EJ (2002) Xyloglucan endotransglycosylases have a function during the formation of secondary cell walls of vascular tissues. Plant Cell **14:** 3073–3088

Bowling AJ, Vaughn KC (2008) Immunocytochemical characterization of tension wood: gelatinous fibers contain more than just cellulose. Am J Bot **95:** 655–663

Bowling AJ, Vaughn KC (2009) Gelatinous fibers are widespread in coiling tendrils and twining vines. Am J Bot **96:** 719–727

Bozzola JJ, Russell LD (1999) Electron Microscopy: Principles and Techniques for Biologists, Ed 2. Jones and Barlett, Boston

Burgert I, Fratzl P (2009) Plants control the properties and actuation of their organs through the orientation of cellulose fibrils in their cell walls. Integr Comp Biol **49:** 69–79

Chang SS, Clair B, Ruelle J, Beauchêne J, Di Renzo F, Quignard F, Zhao GJ, Yamamoto H, Gril J (2009) Mesoporosity as a new parameter for understanding tension stress generation in trees. J Exp Bot **60:** 3023–3030

Chang SS, Quignard F, Alméras T, Clair B (2015) Mesoporosity changes from cambium to mature tension wood: a new step toward the understanding of maturation stress generation in trees. New Phytol **205:** 1277–1287

Clair B, Alméras T, Pilate G, Jullien D, Sugiyama J, Riekel C (2011) Maturation stress generation in poplar tension wood studied by synchrotron radiation microdiffraction. Plant Physiol **155:** 562–570

Clair B, Alméras T, Yamamoto H, Okuyama T, Sugiyama J (2006) Mechanical behavior of cellulose microfibrils in tension wood, in relation with maturation stress generation. Biophys J **91:** 1128–1135

Clair B, Gril J, Di Renzo F, Yamamoto H, Quignard F (2008) Characterization of a gel in the cell wall to elucidate the paradoxical shrinkage of tension wood. Biomacromolecules **9:** 494–498

Clair B, Thibaut B (2001) Shrinkage of the gelatinous layer of poplar and beech tension wood. IAWA J **22:** 121–131

Clair B, Thibaut B, Sugiyama J (2005) On the detachment of the gelatinous layer in tension wood fiber. J Wood Sci **51:** 218–221

Crônier D, Monties B, Chabbert B (2005) Structure and chemical composition of bast fibers isolated from developing hemp stem. J Agric Food Chem **53:** 8279–8289

Decou R, Lhernould S, Laurans F, Sulpice E, Leplé JC, Déjardin A, Pilate G, Costa G (2009) Cloning and expression analysis of a wood-associated xylosidase gene (PtaBXL1) in poplar tension wood. Phytochemistry **70:** 163–172

Dubois M, Gilles KA, Hamilton JK (1956) Colorimetric method for determination of sugars and related substances. Anal Chem **28:** 350–356

Fagerstedt KV, Mellerowicz E, Gorshkova T, Ruel K, Joseleau JP (2014) Cell wall polymers in reaction wood. *In* B Gardiner, J Barnett, P Saranpää, J Gril, eds, Biology of Reaction Wood. Springer-Verlag, Berlin, pp 37–106

Fang CH, Clair B, Gril J, Liu SQ (2008) Growth stresses are highly controlled by the amount of G-layer in poplar tension wood. IAWA J **29:** 237–246

Fournier M, Alméras T, Clair B, Gril J (2014) Biomechanical action and biological functions. *In* B Gardiner, J Barnett, P Saranpää, J Gril, eds, Biology of Reaction Wood. Springer-Verlag, Berlin, pp 139–169

Furuya N, Takahashi S, Miyazaki M (1970) The chemical composition of the gelatinous layer from the tension wood of *Populus euroamericana*. Mokuzai Gakkaishi **16:** 26–30

Gierlinger N, Schwanninger M (2006) Chemical imaging of poplar wood cell walls by confocal Raman microscopy. Plant Physiol **140:** 1246–1254

Gorshkova T, Brutch N, Chabbert B, Deyholos M, Hayashi T, Lev-Yadun S, Mellerowicz EJ, Morvan C, Neutelingsi G, Pilate G (2012) Plant fiber formation: state of the art, recent and expected progress, and open questions. Crit Rev Plant Sci **31:** 201–228

Gorshkova T, Morvan C (2006) Secondary cell-wall assembly in flax phloem fibres: role of galactans. Planta **223:** 149–158

Gorshkova TA, Chemikosova SB, Salnikov VV, Pavlencheva NV, Gurjanov OP, Stolle-Smits T, van Dam JEG (2004) Occurrence of cell-specific galactan is coinciding with bast fibre developmental transition in flax. Ind Crops Prod **19:** 217–224

Gorshkova TA, Gurjanov OP, Mikshina PV, Ibragimova NN, Mokshina NE, Salnikov VV, Ageeva MV, Amenitskii SI, Chernova TE, Chemikosova SB (2010) Specific type of secondary cell wall formed by plant fibers. Russ J Plant Physiol **57:** 328–341

Gorshkova TA, Salnikov VV, Pogodina NM, Chemikosova SB, Yablokova EV, Ulanov AV, Ageeva MV, van Dam JEG, Lozovaya VV (2000) Composition and distribution of cell wall phenolic compounds in the flax (*Linum usitatissimum* L.) stem tissues. Ann Bot (Lond) **85:** 477–486

Gorshkova TA, Wyatt SE, Salnikov VV, Gibeaut DM, Ibragimov MR, Lozovaya VV, Carpita NC (1996) Cell-wall polysaccharides of developing flax plants. Plant Physiol **110:** 721–729

Goswami L, Dunlop JWC, Jungnikl K, Eder M, Gierlinger N, Coutand C, Jeronimidis G, Fratzl P, Burgert I (2008) Stress generation in the tension wood of poplar is based on the lateral swelling power of the G-layer. Plant J **56:** 531–538

Goubet F, Barton CJ, Mortimer JC, Yu X, Zhang Z, Miles GP, Richens J, Liepman AH, Seffen K, Dupree P (2009) Cell wall glucomannan in Arabidopsis is synthesised by CSLA glycosyltransferases, and influences the progression of embryogenesis. Plant J **60:** 527–538

Goubet F, Jackson P, Deery MJ, Dupree P (2002) Polysaccharide analysis using carbohydrate gel electrophoresis: a method to study plant cell wall polysaccharides and polysaccharide hydrolases. Anal Biochem **300:** 53–68

Gurjanov OP, Gorshkova TA, Kabel M, Schols HA, van Dam JEG (2007) MALDI-TOF MS evidence for the linking of flax bast fibre galactan to rhamnogalacturonan backbone. Carbohydr Polym **67:** 86–96

Gurjanov OP, Ibragimova NN, Gnezdilov OI, Gorshkova TA (2008) Polysaccharides, tightly bound to cellulose in the cell wall of flax bast fibre: isolation and identification. Carbohydr Res **72:** 719–729

Hainfeld JF, Powell RD (2000) New frontiers in gold labeling. J Histochem Cytochem **48:** 471–480

Hayashi T, Kaida R, Kaku T, Baba K (2010) Loosening xyloglucan prevents tensile stress in tree stem bending but accelerates the enzymatic degradation of cellulose. Russ J Plant Physiol **57:** 316–320

Hedenström M, Wiklund-Lindström S, Oman T, Lu F, Gerber L, Schatz P, Sundberg B, Ralph J (2009) Identification of lignin and polysaccharide modifications in *Populus* wood by chemometric analysis of 2D NMR spectra from dissolved cell walls. Mol Plant **2:** 933–942

Ibatullin FM, Banasiak A, Baumann MJ, Greffe L, Takahashi J, Mellerowicz EJ, Brumer H (2009) A real-time fluorogenic assay for the visualization of glycoside hydrolase activity in planta. Plant Physiol **151:** 1741–1750

Jensen MH, Otten H, Christensen U, Borchert TV, Christensen LLH, Larsen S, Leggio LL (2010) Structural and biochemical studies elucidate the mechanism of rhamnogalacturonan lyase from *Aspergillus aculeatus*. J Mol Biol **404:** 100–111

Jones L, Seymour GB, Knox JP (1997) Localization of pectic galactan in tomato cell walls using a monoclonal antibody specific to (1→4)-β-D-galactan. Plant Physiol **113:** 1405–1412

Joseleau JP, Imai T, Kuroda K, Ruel K (2004) Detection *in situ* and characterization of lignin in the G-layer of tension wood fibres of *Populus deltoides*. Planta **219:** 338–345

Kaku T, Serada S, Baba K, Tanaka F, Hayashi T (2009) Proteomic analysis of the G-layer in poplar tension wood. J Wood Sci **55:** 250–257

Kim JS, Daniel G (2012) Distribution of glucomannans and xylans in poplar xylem and their changes under tension stress. Planta **236:** 35–50
Knox JP, Linstead PJ, Peart J, Cooper C, Roberts K (1991) Developmentally regulated epitopes of cell surface arabinogalactan proteins and their relation to root tissue pattern formation. Plant J **1:** 317–326
Kudla J, Batistic O, Hashimoto K (2010) Calcium signals: the lead currency of plant information processing. Plant Cell **22:** 541–563
Kuo CM, Timell TE (1969) Isolation and characterization of a galactan from tension wood of American beech (*Fagus grandifolia* Ehrl.). Svensk Papperstidn **72:** 703–716
Lafarguette F, Leplé JC, Déjardin A, Laurans F, Costa G, Lesage-Descauses MC, Pilate G (2004) Poplar genes encoding fasciclin-like arabinogalactan proteins are highly expressed in tension wood. New Phytol **164:** 107–121
Lamport DT, Várnai P (2013) Periplasmic arabinogalactan glycoproteins act as a calcium capacitor that regulates plant growth and development. New Phytol **197:** 58–64
Love GD, Snape CE, Jarvis MC, Morrison IM (1994) Determination of phenolic structures in flax fibre by solid state ^{13}C NMR. Phytochemistry **35:** 489–492
Marcus SE, Blake AW, Benians TAS, Lee KJ, Poyser C, Donaldson L, Leroux O, Rogowski A, Petersen HL, Boraston A, et al (2010) Restricted access of proteins to mannan polysaccharides in intact plant cell walls. Plant J **64:** 191–203
Marcus SE, Verhertbruggen Y, Hervé C, Ordaz-Ortiz JJ, Farkas V, Pedersen HL, Willats WGT, Knox JP (2008) Pectic homogalacturonan masks abundant sets of xyloglucan epitopes in plant cell walls. BMC Plant Biol **8:** 60–71
McCartney L, Marcus SE, Knox JP (2005) Monoclonal antibodies to plant cell wall xylans and arabinoxylans. J Histochem Cytochem **53:** 543–546
Meier H (1962) Studies on galactan from tension wood of beech (*Fagus silvatica* L.). Acta Chem Scand **16:** 2275–2283
Mellerowicz EJ, Baucher M, Sundberg B, Boerjan W (2001) Unravelling cell wall formation in the woody dicot stem. Plant Mol Biol **47:** 239–274
Mellerowicz EJ, Gorshkova TA (2012) Tensional stress generation in gelatinous fibres: a review and possible mechanism based on cell-wall structure and composition. J Exp Bot **63:** 551–565
Mellerowicz EJ, Immerzeel P, Hayashi T (2008) Xyloglucan: the molecular muscle of trees. Ann Bot (Lond) **102:** 659–665
Mikshina PV, Chemikosova SB, Mokshina NE, Ibragimova NN, Gorshkova TA (2009) Free galactose and galactosidase activity in the course of flax fiber development. Russ J Plant Physiol **56:** 58–67
Mikshina PV, Gurjanov OP, Mukhitova FK, Petrova AA, Shashkov AS, Gorshkova TA (2012) Structural details of pectic galactan from the secondary cell walls of flax (*Linum usitatissimum* L.) phloem fibres. Carbohydr Polym **87:** 853–861
Mikshina PV, Idiyatullin BZ, Petrova AA, Shashkov AS, Zuev YF, Gorshkova TA (2015) Physicochemical properties of complex rhamnogalacturonan I from gelatinous cell walls of flax fibers. Carbohydr Polym **117:** 853–861
Mizrachi E, Maloney VJ, Silberbauer J, Hefer CA, Berger DK, Mansfield SD, Myburg AA (2014) Investigating the molecular underpinnings underlying morphology and changes in carbon partitioning during tension wood formation in *Eucalyptus*. New Phytol **206:** 1351–1363
Mokshina NE, Ibragimova NN, Salnikov VV, Amenitskii SI, Gorshkova TA (2012) Galactosidase of plant fibers with gelatinous cell wall: identification and localization. Russ J Plant Physiol **59:** 246–254
Müller M, Burghammer M, Sugiyama J (2006) Direct investigation of the structural properties of tension wood cellulose microfibrils using microbeam x-ray fibre diffraction. Holzforschung **60:** 474–479
Nishikubo N, Awano T, Banasiak A, Bourquin V, Ibatullin F, Funada R, Brumer H, Teeri TT, Hayashi T, Sundberg B, et al (2007) Xyloglucan endo-transglycosylase (XET) functions in gelatinous layers of tension wood fibers in poplar: a glimpse into the mechanism of the balancing act of trees. Plant Cell Physiol **48:** 843–855
Norberg PH, Meier H (1966) Physical and chemical properties of gelatinous layer in tension wood fibres of aspen (*Populus tremula* L.). Holzforsehung **20:** 174–178
Olsson AM, Bjurhager I, Gerber L, Sundberg B, Salmén L (2011) Ultrastructural organisation of cell wall polymers in normal and tension wood of aspen revealed by polarisation FTIR microspectroscopy. Planta **233:** 1277–1286
Pattathil S, Avci U, Baldwin D, Swennes AG, McGill JA, Popper Z, Bootten T, Albert A, Davis RH, Chennareddy C, et al (2010) A comprehensive toolkit of plant cell wall glycan-directed monoclonal antibodies. Plant Physiol **153:** 514–525
Paux E, Carocha V, Marques C, Mendes de Sousa A, Borralho N, Sivadon P, Grima-Pettenati J (2005) Transcript profiling of *Eucalyptus* xylem genes during tension wood formation. New Phytol **167:** 89–100
Pilate G, Dejardin A, Laurans F, Leple JC (2004) Tension wood as a model for functional genomics of wood formation. New Phytol **164:** 63–72
Ralet MC, Tranquet O, Poulain D, Moïse A, Guillon F (2010) Monoclonal antibodies to rhamnogalacturonan I backbone. Planta **231:** 1373–1383
Reynolds ES (1963) The use of lead citrate at high pH as an electron-opaque stain in electron microscopy. J Cell Biol **17:** 208–212
Roach MJ, Deyholos MK (2007) Microarray analysis of flax (*Linum usitatissimum* L.) stems identifies transcripts enriched in fibre-bearing phloem tissues. Mol Genet Genomics **278:** 149–165
Roach MJ, Mokshina NY, Badhan A, Snegireva AV, Hobson N, Deyholos MK, Gorshkova TA (2011) Development of cellulosic secondary walls in flax fibers requires β-galactosidase. Plant Physiol **156:** 1351–1363
Ruel K, Barnoud F (1978) Research on the quantitative determination of tension wood in beech: statistical significance of the galactose content. Holzforschung **32:** 149–156
Rüggeberg M, Saxe F, Metzger TH, Sundberg B, Fratzl P, Burgert I (2013) Enhanced cellulose orientation analysis in complex model plant tissues. J Struct Biol **183:** 419–428
Salmén L, Burgert I (2009) Cell wall features with regard to mechanical performance: a review. Holzforschung **63:** 121–129
Salnikov VV, Ageeva MV, Gorshkova TA (2008) Homofusion of Golgi secretory vesicles in flax phloem fibers during formation of the gelatinous secondary cell wall. Protoplasma **233:** 269–273
Sandquist D, Filonova L, von Schantz L, Ohlin M, Daniel G (2010) Microdistribution of xyloglucan in differentiating poplar cells. BioResources **5:** 796–807
Schreiber N, Gierlinger N, Pütz N, Fratzl P, Neinhuis C, Burgert I (2010) G-fibres in storage roots of Trifolium pratense (Fabaceae): tensile stress generators for contraction. Plant J **61:** 854–861
Takata R, Tokita K, Mori S, Shimoda R, Harada N, Ichinose H, Kaneko S, Igarashi K, Samejima M, Tsumuraya Y, et al (2010) Degradation of carbohydrate moieties of arabinogalactan-proteins by glycoside hydrolases from *Neurospora crassa*. Carbohydr Res **345:** 2516–2522
Talmage KW, Keegstra K, Bauer WO, Albersheim P (1973) The structure of plant cell walls: I. The macromolecular components of the walls of suspension-cultured sycamore cells with a detailed analysis of the pectic polysaccharides. Plant Physiol **51:** 158–173
Tan L, Varnai P, Lamport DTA, Yuan C, Xu J, Qiu F, Kieliszewski MJ (2010) Plant O-hydroxyproline arabinogalactans are composed of repeating trigalactosyl subunits with short bifurcated side chains. J Biol Chem **285:** 24575–24583
Tryfona T, Liang HC, Kotake T, Tsumuraya Y, Stephens E, Dupree P (2012) Structural characterization of Arabidopsis leaf arabinogalactan polysaccharides. Plant Physiol **160:** 653–666
Tsumuraya Y, Mochizuki N, Hashimoto Y, Kovác P (1990) Purification of an exo-β-(1→3)-D-galactanase of Irpex lacteus (Polyporus tulipiferae) and its action on arabinogalactan-proteins. J Biol Chem **265:** 7207–7215
Wardrop AB, Dadswell HE (1948) The nature of reaction wood. I. The structure and properties of tension wood fibres. Aust J Sci Res Ser B **1:** 4–19
Yamamoto H, Abe K, Arakawa Y, Okuyama T, Gril J (2005) Role of the gelatinous layer (G-layer) on the origin of the physical properties of the tension wood of *Acer sieboldianum*. J Wood Sci **51:** 222–233
Yamamoto H, Ruelle J, Arakawa Y, Yoshida M, Clair B, Gril J (2009) Origin of the characteristic hygro-mechanical properties of gelatinous layer in tension wood from Kunugi oak (*Quercus acutissima*). Wood Sci Technol **44:** 149–163